Remote Sensing of Environment 326 (2025) 114798

Contents lists available at ScienceDirect

Remote Sensing of Environment

journal homepage: www.elsevier.com/locate/rse

Kinematic inventory of rock glaciers in the Pyrenees based on InSAR and airborne LiDAR data

Jesús Guerrero [a,*], Miguel Guerra [a], Thiery Yannick [b], Gloria Desir [a], Bastien Colas [c]

[a] University of Zaragoza, Earth Science Department, Spain
[b] Bureau de Recherche Géologique et Minières, DRP, R3C, Europarc, France
[c] Bureau de Recherche Géologique et Minières Occitanie, Site de Montpellier, France

ARTICLE INFO

Edited by Jing M. Chen

Keywords:
SqueeSAR
Permafrost degradation
Frozen ground
Rock glacier database
Axial Pyrenees
Periglacial

ABSTRACT

Rock glaciers (RGs) are ice and debris landforms shaped by long-term permafrost creep. Their inventory has expanded significantly in the past two decades due to their importance as water resources and indicators of climate change. Previous inventories in the Pyrenees are sparse and lack essential kinematic data, leading to an underestimation of active RGs. This study presents the first kinematic database of Pyrenean RGs, integrating European Ground Motion Service (EGMS) InSAR data with airborne Laser Imaging Detection and Ranging (LiDAR) datasets and seven years of Sentinel-1 high-resolution InSAR data processed by the SqueeSAR algorithm. The analysis focuses on three igneous plutons (Panticosa, Cauterets, and Neouvielle) in the central Pyrenees, comparing surface displacement rates from these techniques to previous geodetic measurements. A total of 733 RGs have been mapped in the Pyrenees, covering an area of 58.9 km^2. 73 % of the mapped RGs are inactive or relict, showing no ground displacement and being partially vegetated. Only 13 % (96 RGs) remain active, covering less than 10 km^2, and are primarily north-facing. An additional 14 % (102 RGs) lack InSAR data but they are considered potentially active based on their orientation, altitude, and remarkable morphological features. The existence of active RGs at relatively low altitudes lowers the permafrost boundary between 2100 and 2600 m on north- and south-facing slopes, respectively. Despite the limitations of InSAR to measure displacements along the north-south axis and the fact that most active RGS are oriented to the north, according to the decomposition of the LOS displacement to vertical and horizontal components and LiDAR data, the ongoing subsidence and decline in horizontal movement related to ice degradation suggest a transition of many RGs from active to relict, marking rapid permafrost degradation. Finally, the EGMS has proven inadequate for detecting slow-moving active RGs in the Pyrenees due to temporal decorrelation caused by prolonged snow cover periods, particularly when compared to the combined use of SqueeSAR and airborne LiDAR datasets. The EGMS detected ground information for only 14 out of 89 active RGs, provided inaccurate kinematic data and underestimated the decomposed vertical and horizontal velocities by up to fourfold.

1. Introduction

Rock glaciers (RGs) are periglacial landforms, either lobate or tongue-shaped, composed of ice and debris, characterized by a frontal slope, lateral margins, and a distinctive ridge-and-furrow surface morphology, which results from long-term permafrost creep (White, 1976; Barsch, 1992; Berthling, 2011). Over the past two decades, the number of RG inventories has increased significantly due to their hydrological importance as water resources in arid and semiarid regions (Jones et al., 2018), and their value as indicators of mountain permafrost, serving as sensitive markers of climate change (Bertone et al., 2022). As a result, RGs have been extensively studied in the Arctic and sub-Arctic regions (Serrano, and López-Martínez, J., 2000; Lilleøren et al., 2022), as well as in many high mountain ranges worldwide, including the Himalayas (Wang et al., 2017; Cai et al., 2021; Hu et al., 2023), the Rocky Mountains (Munroe, 2018; Johnson et al., 2021), the Andes (Villarroel et al., 2018; Zalazar et al., 2020), and the Alps (Colucci et al., 2016; Wagner et al., 2020).

In the Pyrenees, active RGs are frequently found above 2600 m (Martinez de Pison et al., 1998; Serrano et al., 1999), but their inventory

* Corresponding author.
E-mail addresses: jgiturbe@unizar.es (J. Guerrero), m.guerra@unizar.es (M. Guerra), Y.Thiery@brgm.fr (T. Yannick), gdesir@unizar.es (G. Desir), b.colas@brgm.fr (B. Colas).

https://doi.org/10.1016/j.rse.2025.114798
Received 13 January 2025; Received in revised form 25 February 2025; Accepted 3 May 2025
Available online 8 May 2025

remains sparse in the Spanish side (Serrano et al., 2011; García-Ruiz et al., 2011; Gómez Ortiz et al., 2011; Fernandes et al., 2017; Ventura, 2020) and even more limited in the French side (Cazenave-Piarrot and Tihay, 1983; Cazenave-Piarrot and Tihay, 1986; Serrano et al., 2011; Feuillet and Mercier, 2012; Ventura, 2016). In addition, none of the previous regional inventories include information related to their kinematics which is necessary to classify them as active, non-active and relict as recommended by the guidelines of the International Permafrost Association (IPA) Action Group (RGIK, 2023). Consequently, the velocity and dynamics of RGs in the Pyrenees remains poorly understood with only five RGs are known to be active based on the use of GNSS and in-situ geomatics techniques (Serrano et al., 1999; Chueca and Julián, 2005; Serrano et al., 2006, 2010; González-García et al., 2013; de Sanjosé et al., 2014; Martínez-Fernández et al., 2024). This underestimation highlights the need for a comprehensive RG inventory at a regional scale, providing detailed information on their location and activity. This inventory will provide a more detailed characterization of the spatial and altitudinal distribution of permafrost in the Pyrenees and elucidate its current dynamics in order to assess the impact of climate change on its degradation.

To address this gap, multi-temporal Interferometric Synthetic Aperture Radar (MTInSAR) has been proven a powerful technique and a reliable method for the remote detection of active RGs and the quantification of their surface displacement (Liu et al., 2013; Wang et al., 2017; Cai et al., 2021; Bertone et al., 2022; Reinosch et al., 2021; Zhang et al., 2021; Hu et al., 2023) even at velocities lower than 1 cm/yr (Strozzi et al., 2020; Lilleøren et al., 2022). In this context, the European Space Agency (ESA) launched the European Ground Motion Service (EGMS) in May 2022, offering precise, free-access Sentinel-1 differential InSAR (DinSAR) data for non-expert users to detect ground movements across Europe with millimetre-level precision (Crosetto et al., 2020; Crosetto et al., 2021; Constantini et al., 2021; EGMS, 2023). While this space-borne radar database has been successfully applied for monitoring landslides, subsidence, earthquakes, and volcanic phenomena (Constantini et al., 2021; Sala Calero et al., 2023), its efficacy in detecting active RGs has yet to be demonstrated.

This study presents the most recent and comprehensive RG database for the Pyrenees, encompassing the entire range and including kinematic data derived from velocity maps provided by the EGMS InSAR dataset. In order to assess the efficiency and accuracy of this online platform for RGs inventories, the resulting surface displacement maps are compared with the ones obtained by the multi-technique integration of airborne LiDAR (Laser Imaging Detection and Ranging) point clouds acquired in 2010 and 2020 and 7-year Sentinel-1 InSAR data at full resolution in ascending and descending orbits processed by the commercial software SqueeSAR, focusing on three igneous plutons in the central western Pyrenees (Fig. 1). Lastly, we discuss the current permafrost distribution based on the altitude and orientation of active RGs, compare their

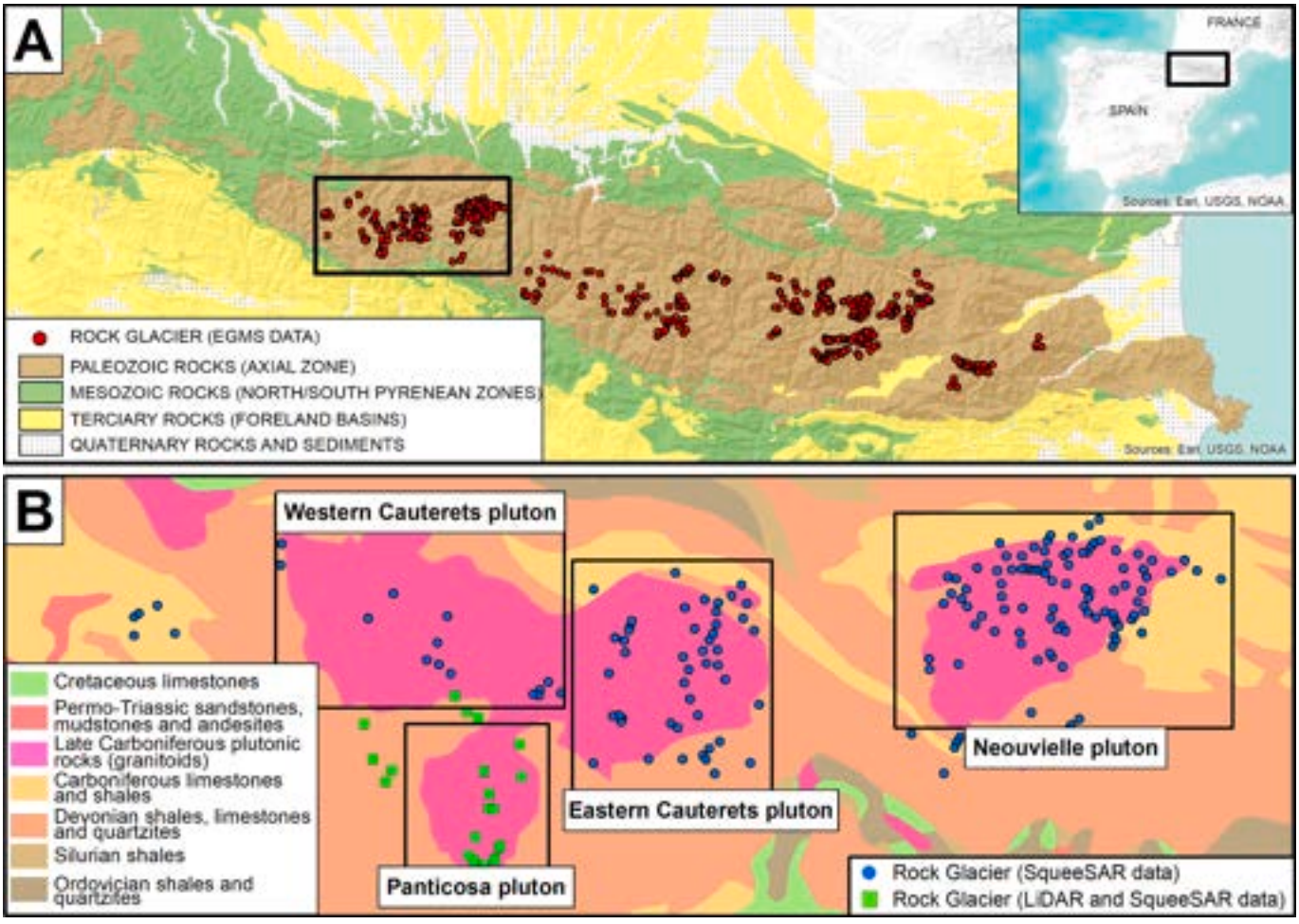

Fig. 1. (A) Geographical location and geological map of the Pyrenees depicting the larger RGs whose creep rates have been derived from the EGMS dataset. The black box, that is zoomed in the lower image, delineates the area used for the EGMS data analysis by LiDAR and the SqueeSAR algorithm. (B) Geological sketch of the central axial Pyreenes showing the prevailing location of RGs in the westernmost igneous plutons. The green squares indicate rock glaciers identified using a combination of LiDAR and SqueeSAR data. The blue dots represent rock glaciers detected solely using SqueeSAR data. (For interpretation of the references to colour in this figure legend, the reader is referred to the web version of this article.)

movement rates with previous geomatics studies and analyse their future scenario in response to global warming.

2. Study area (geology, geomorphology (glacial and permafrost history/current situation) and climatology

The Pyrenees is an alpine, narrow, NNW-SSE oriented mountain range that serves as a natural boundary between Spain, France and Andorra (Fig. 1). The range was formed as a result of the convergence between the Iberian and European tectonic plates, spanning from the Late Cretaceous to the Miocene (Muñoz, 2002). Its structure is rather simple and can be divided into three main structural domains (e.g. Barnolas and Pujalte, 2004). These domains consist of a central Paleozoic basement outcrop, referred to as the Axial Zone, flanked by two fold-and-thrust belt units comprising Mesozoic and Tertiary rocks to the north and south, known as the North-Pyrenean and South-Pyrenean Zones, respectively (Fig. 1A).

The Axial Zone is characterized by numerous Late Hercynian calc-alkaline plutons intruded into highly deformed Paleozoic sedimentary and metamorphic rocks (Santana Torre, 2002). The westernmost igneous massifs include the Panticosa-Cauterets complex and the Neouvielle pluton (Fig. 1B). The Panticosa-Cauterets complex comprises the syntectonic Panticosa, Western Cauterets, and Eastern Cauterets plutons, which were emplaced during the D2 Variscan tectonic phase in a transpressive regime into Devonian and Carboniferous shales, limestones, and quartzites (Santana Torre, 2002). These plutons exhibit concentric compositional zoning, transitioning from tonalites at the margins to granodiorites and monzogranites towards the center (Galé, 2005). Additionally, Permian mafic dykes cut through both the pluton and surrounding country rocks (Gil et al., 2012). The Neouvielle massif, with a triangular shape, displays a high-K calc-alkaline geochemical signature and consists of monzogranites at its core and granodiorites at its periphery (Gleizes et al., 2001). The surrounding country rocks, metamorphosed to greenschist facies, are composed of Devonian shales, sandstones, limestones, and quartzites, as well as Carboniferous shales and limestones (Lemirre et al., 2019).

The Pyrenees have been shaped by glacial phases spanning the Late Pleistocene to the Holocene, resulting in a range of erosional and depositional glacial landforms, such as arêtes, cirques, horns, and deep glacial valleys bordered by lateral and frontal moraines, as well as steep slopes. Optically stimulated luminescence (OSL) and cosmic-ray exposure (CRE) dating of moraines, boulders, fluvioglacial and landslide-dam deposits have provided insights into the glacial history of the Pyrenees (Andrés et al., 2018 and references therein; Turu et al., 2023 and references therein). The glacial evolution can be summarized as follows: (1) an early glacial cycle during Marine Oxygen Isotope Stage (MIS) 6, around 150 ka, (2) maximum ice extent (MIE) during MIS 4, approximately 65 ka, (3) the global Last Glacial Maximum (LGM) around 25 ka, (4) rapid glacial retreat post-LGM, punctuated by advances during the Older (17.5–14.5 ka) and Younger Dryas (12.9–11.7 ka), and (5) near-complete deglaciation of most cirques by the end of the Younger Dryas and Early Preboreal (10 ka), with glacier disappearance occurring during the Holocene Thermal Maximum (7–5.5 ka).

CRE dating of relict RGs boulders throughout the range suggests that these landforms primarily developed during the Bølling–Allerød interstadial or shortly after the Younger Dryas, as a natural transition from glacial to periglacial conditions (Palacios et al., 2015, 2017; Andrés et al., 2018). This period marked the evolution from debris-free glaciers to debris-covered glaciers, and finally to RGs (Fernandes et al., 2023). Some RGs at the highest summits likely remained active until the Holocene Thermal Optimum (Palacios et al., 2015) and some might persisted to the early Holocene (Serrano et al., 2010; García-Ruiz et al., 2014), owing to the insulating effect of large block and boulder masses. The Little Ice Age (LIA) (14th to 19th centuries) represents the most recent cold period following the Younger Dryas-Holocene transition, during which small glaciers reformed at the highest summits (Oliva et al., 2019). Since 1850, these glaciers have been receding, with accelerated shrinkage observed from the late 20th century onward (Vidaller et al., 2021, 2023). Today, only 19 small glaciers remain, with a maximum thickness of 45 m and a total area of 2.42 km^2 (Rico, 2019). Based on current rates of glacial retreat and the progressive temperature increase recorded over the past 60 years (OPCC, 2024), it is projected that Pyrenean glaciers may completely disappear within the next 20 years (Vidaller et al., 2021). Consequently, it is reasonable to infer that the disappearance of current glaciers will also mark the end of activity for the few RGs that remain active today. Current knowledge of frozen ground distribution in the Pyrenees remains limited, with most available data derived from localized studies of periglacial landforms, such as patterned grounds (Feuillet and Mercier, 2012), frost mounds (Serrano et al., 2010; González-García et al., 2016a), protalus ramparts (González-García et al., 2016b) and active RGs situated at elevations above 2600 m a.s.l (Serrano et al., 1999; Chueca and Julián, 2005; Serrano et al., 2006, 2010; González-García et al., 2013; de Sanjosé et al., 2014; Martínez-Fernández et al., 2024). However, the measurements of basal snow cover temperatures (Julián and Chueca, 2007), indicates the potential existence of permafrost at lower altitudes.

The climate of the Pyrenees is highly variable, with a pronounced west–east gradient in temperature and moisture. The western and north-facing slopes are characterized by an Atlantic climate, with mild temperatures and annual precipitation exceeding 2000 mm. In contrast, the eastern and south-facing slopes experience a Mediterranean climate, with higher temperatures and annual precipitation as low as 600 mm in the driest regions (Del Barrio et al., 1990; Serrano et al., 2018). The 0 °C isotherm ranges from 2700 to 3000 m in elevation from west to east, and snowpack above 2000 m typically persists for six months (López-Moreno et al., 2020 and references therein). In this context, the Panticosa, Cauterets, and Neouvielle plutons host numerous peaks that rise above the 0 °C isotherm, with elevations ranging from 2700 to 3150 m. The Panticosa pluton, located on the southern slope of the range, receives approximately 1500 mm of annual rainfall, with an average annual temperature of 8 °C at 1000 m. In contrast, the Cauterets and Neouvielle plutons, located on the northern slopes, receive an additional 500–1000 mm of rainfall and exhibit temperatures 3–4 °C lower than the Panticosa massif at equivalent altitudes (Feuillet, 2010).

3. Methodology

3.1. Inventory

The geomorphological mapping of RGs was performed manually by their distinct ridge and swale surface topography using high resolution orthoimages taken in 1956 and 2021 and a 5 m spatial resolution digital elevation model (DEM) downloaded from the Spanish and French National Cartographic Institutes (IGN and RGE, respectively) and Google Earth Pro that provides access to multiples three-dimensional images of the same location at different years. The database was complemented with Basemap Esri images and later integrated in a GIS environment. Their topographical and morphometric parameters (maximum and minimum altitude, slope, length, width and area) were extracted from the DEM.

3.2. Techniques (InSAR, EGMS, LiDAR)

The detection of active RGs was determined from the EGMS InSAR dataset. The EGMS viewer, which is included in the Copernicus Land Monitoring Service, freely distributes consistent and reliable LOS displacement maps in ascending and descending orbits and decomposed vertical (Vv) and horizontal (Vh) components products resampled to a 100 m grid, covering the complete period between 2015 and 2022 all over Europe. Ground measuring points are derived from the advanced DiNSAR processing of Sentinel-1 images at full resolution using Permanent Scatterers (PS) and Distributed Scatterers (DS). The key

elements of the EGMS are outlined in the White Paper (EGMS, 2017), and the implementation plan and product specification document (EGMS, 2020). A review of the technical approaches employed by the EGMS are described in Crosetto et al. (2021) and Ferretti et al. (2021).

The EGMS velocity maps were validated in three granodioritic plutons (Panticosa, Cauterets, and Neouvielle) using airborne LiDAR data and high-resolution InSAR data processed with the SqueeSAR algorithm. The airborne LiDAR data, covering only the Spanish territory, were freely accessed from the IGN public server. Point clouds were acquired in January 2010 and July 2020 (a span of 3842 days; 10.52 years), using Leica ALS-60 and ALS-80 laser scanners from an aircraft at an altitude of 3500 m (Lorite Martínez et al., 2016). The ground point density exceeded 0.5 points/m^2, with mean square errors of 20 cm and 10 cm in the vertical and horizontal axes, respectively. Co-registration errors in stable areas on steep slopes ranged from 80 to 100 cm. Thus, considering the vertical, horizontal, and co-registration errors, only RGs with a mean displacement rate exceeding 10 cm/yr (100 cm over 10 years) could be confidently detected. Point clouds were aligned and compared in 3D using the CloudCompare software and the M3C2 algorithm (Lague et al., 2013), following the procedures outlined by Zahs et al. (2019) and Sevil Aguareles et al. (2021). It is pertinent to mention that the European Ground Motion Service (EGMS) exhibits a lack of ground deformation data in the Andorran Pyrenees, resulting in a significant data deficit.

A total of 886C-band Sentinel-1 IW mode Single Look Complex images, with a resolution of 5 × 20 m and 6-day temporal baselines, were acquired in ascending and descending geometries from May 2015 to September 2021. These were processed using the commercial SqueeSAR algorithm (Ferretti et al., 2011) to generate ground deformation maps for the Panticosa, Cauterets, and Neouvielle plutons. To reduce noise and avoid temporal and volumetric decorrelation due to snow cover (Klees and Massonnet, 1998; Bertone et al., 2022), only snow-free periods (from mid-May to mid-December) were considered. The SqueeSAR method analyzes entire stacks of SAR images, identifying and combining PS and DS to overcome the low density of PS in natural areas, thus maximizing the spatial density of measurement points (Ferretti et al., 2011; Nardini et al., 2024). This technique measures surface displacement along the satellite LOS with millimetric accuracy (Colesanti et al., 2003). In accordance to the EGMS framework (Crosetto et al., 2020) and assuming that the north-south component is almost negligible due to the near-insensitivity of InSAR to motion in that direction (Bru et al., 2024), the decomposed horizontal (Vh) and vertical (Vv) velocities were derived by combining ascending and descending data using the method described by Notti et al. (2014). Later, the resulting displacement maps were classified according to the mean decomposed vertical and horizontal deformation velocities. The green colour reflects motionless areas and deformation rates between +3.0 and − 3.0 mm/yr (sensitivity of the SqueeSAR technique) (Nardini et al., 2024) while the colour gradients from yellow to red and from blue to violet represent increasing deformation rates. Lastly, the decomposed vertical and horizontal displacement time series (TS) were plotted from all the moving points of each RG to assess temporal average movement patterns and compare the SqueeSAR and EGMS datasets.

3.3. Classification

RGs were classified according to the traditional geomorphological framework proposed by Barsch (1992), rather than the kinematic classification advocated by the International Permafrost Association (IPA) Action Group (RGIK, 2023). This approach was adopted because the EGMS is lacking movement data for a substantial number of RGs and the absence of any relevant data for the Andorra region. Based on their geomorphological features and available InSAR data, RGs were categorized into four categories: active (coherent movement across most of the surface, with steep front slopes and prominent ridges and furrows), possibly active (no InSAR data but significant topographical features, appropriate altitude and orientation, and occasionally literature evidence of movement), inactive (InSAR displacement less than 3 mm/yr movement but fresh-looking geometry and minimal vegetation cover), and relict (InSAR displacement less than 3 mm/yr, substantial vegetation cover, thermokarst structures, and an incised drainage network).

4. RGs inventory in the Pyrenees

A total of 733 RGs have been mapped across the entire study area. Their geographical locations are provided in a point-type KML file, available as supplementary material. They cover an area of 58.9 km^2 and are situated at average slopes of 14 degrees and elevations between 1288 and 3062 m with an average altitude of around 2400 (Table 1). This elevation range results in the majority of RGs being located within the axial zone (Fig. 1), which contains the highest peaks, with over 150 summits exceeding 3000 m in altitude. The equilibrium line altitude of the remaining glaciers is situated around 3100 m (Campos et al., 2021). The morphometric characteristics of the RGs exhibit high variability, with maximum, minimum, and average widths of 885 m, 28 m, and 210 m, respectively, and maximum, minimum, and average lengths of 2758 m, 52 m, and 484 m, respectively. Most RGs (66 %) are found in highly fractured Paleozoic granodioritic batholiths and volcanic rocks, while 31 % occur in metamorphic rocks, both of which provide significant quantities of gelifracts. As a result, RGs in igneous rocks exhibit greater lengths and cover larger areas (Fig. 2A). A smaller proportion (3 %) are located in sedimentary rocks, primarily limestone. Following the classifications proposed by Barsch (1992), Berthling (2011), and Pandey (2019), as well as previous inventories (Serrano et al., 2011; García-Ruiz et al., 2011; Gómez Ortiz et al., 2011; Fernandes et al., 2017; Ventura, 2020), the RGs were categorized into two types: (1) talus-type RGs, which are associated with talus slopes originating from steep headwalls and are characterized by interstitial ice, and (2) moraine-type RGs, which are located between the inner frontal moraine and the cirque walls and are likely the result of the natural evolution of debris-covered glaciers. Talus-type RGs constitute 38 % (277) of the total, while moraine-type RGs represent 62 % (456). With respect to their orientation, the RGs are predominantly oriented towards the north, with significantly fewer RGs facing NE or NW, indicating that northern slopes were more favourable for RG formation in the past due to reduced solar radiation and mean temperature, coupled with greater snow cover thickness and persistence (Fig. 2B).

Today, based on InSAR data, 73 % of the Pyrenean RGs (536 out of 733) are classified as inactive or relict, with ground displacement less than 3 mm/yr. These RGs exhibit complete or partial vegetation cover and are degraded by the drainage network. Only 13 % (96 out of 733) remain active, covering an area of less than 10 km2. The active RGs predominantly face north (49), northeast (16), or northwest (13) slopes, with a smaller number oriented towards the east (5), southeast (3), southwest (3), and west (7); none are oriented to the south (Table 1, Fig. 2). The majority of the active RGs are moraine-type (66 %), with lengths and widths ranging from several tens to hundreds of meters. They are primarily located at the base of vertical headwall cirques, at elevations exceeding 2000 m. An additional 14 % of RGs (102 out of 733) lack InSAR data and have been classified as possibly active based on their northern orientation, high altitude, and relatively fresh geomorphological appearance (Table 1).

5. RGs kinematics and movement characterization in the central western Pyrenees

The mean decomposed vertical and horizontal displacement rates of 96 active RGs in Panticosa, Cauterets and Neouville granodioritic plutons were calculated using LiDAR and SAR imagery processed with the SqueeSAR commercial software (Fig. 1B). The following subsections describe the location, kinematic status, and decomposed vertical and horizontal velocities of these RGs, along with the detection rates

Table 1
Statistical summary of rock glaciers (RGs) in the Pyrenees. Values for active RGs are highlighted in red.

ACTIVITY	TYPE	LITHOLOGY	ORIENTATION	WIDTH (m)	LENGTH (m)	ALTITUDE (m)	SLOPE (°)	AREA (Km2)
ACTIVE (96/13 %)		Limestone (17/**4**)	N (276/**49**)					Min = 6.9 *10^{-4}
POSIBLY ACTIVE (102/14 %)		Metamorphic rocks (232/**12**)	NE-NW (193/**29**)	Min = 28 (**32**)	Min = 52 (**69**)	Min = 1288 (**2010**)	Min = 4 (**3**)	Max = 0.9
INACTIVE (265/36 %)			E-W (144/**12**)					Av = 0.08
			SE-SW (76/**6**)	Max = 885 (**743**)	Max = 2758 (**1525**)	Max = 3062 (**2914**)	Max = 35 (**33**)	
RELICT (271/37 %)	Moraine (456/**64**) Talus (277/**32**)	Igneous rocks (484/**80**)	S (44/**0**)	Av = 210 (**227**)	Av = 484 (**532**)	Av = 2346 (**2404**)	Av = 14 (**13**)	Total = 58.9 (**9.4**)

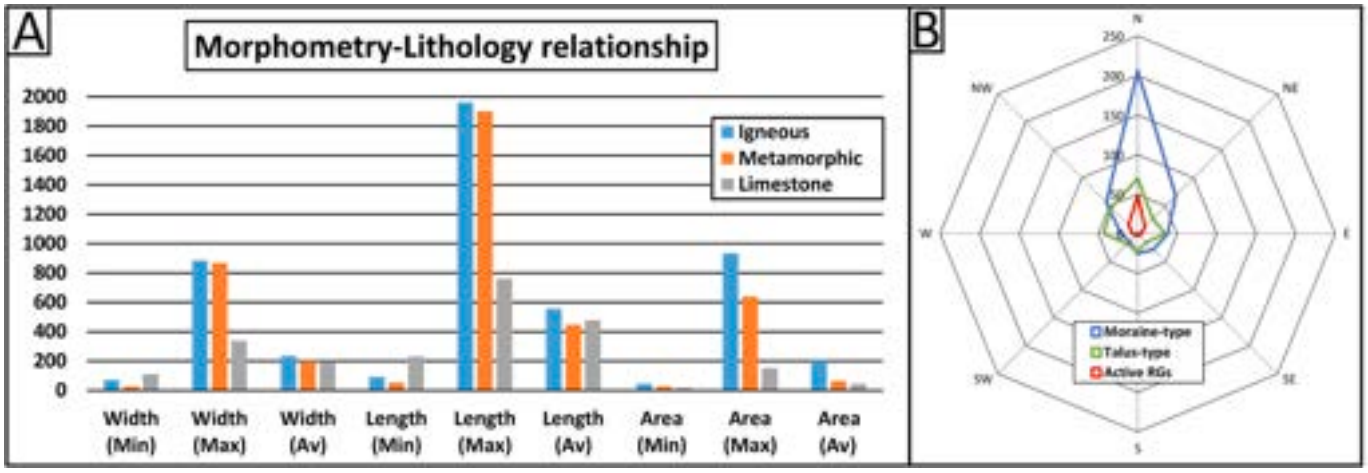

Fig. 2. (A) Morphometric parameters depending on the lithology of the source area of the debris. (B) Aspect angle plots of moraine-type, talus-type and active RGs preferably facing north.

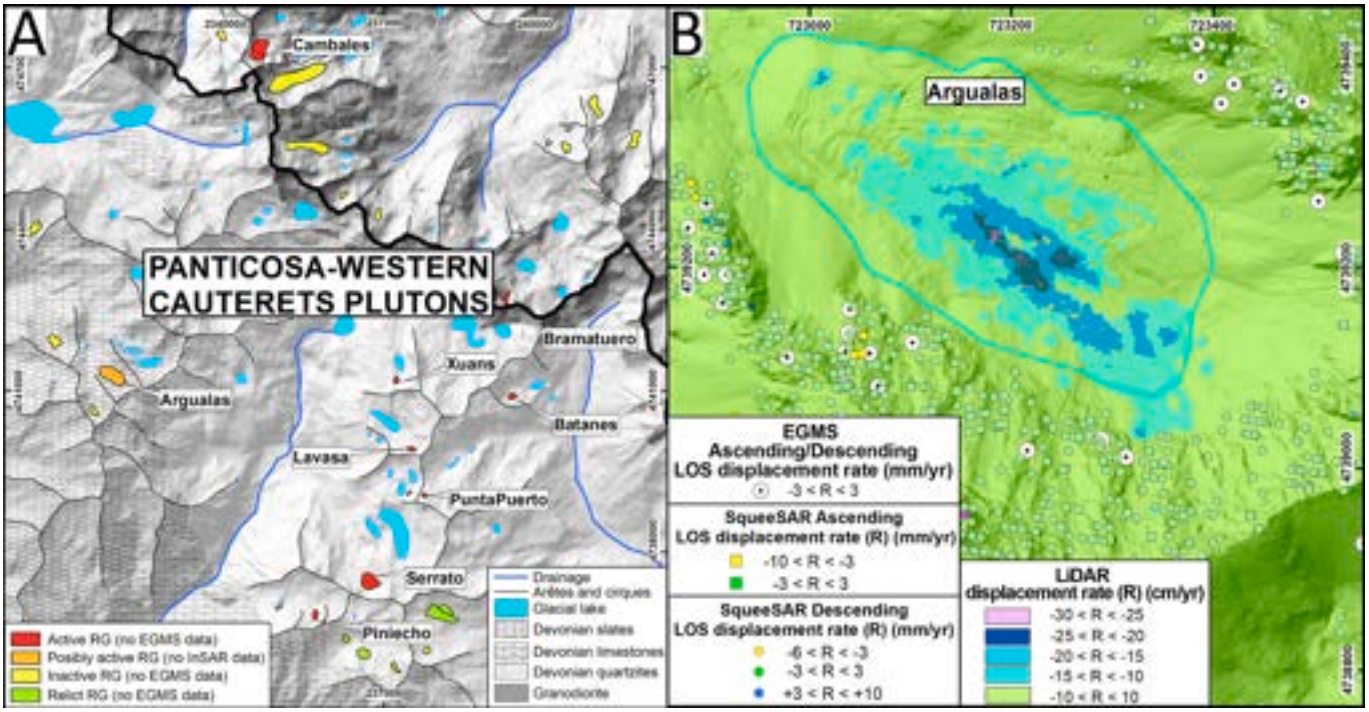

Fig. 3. (A) Geological sketch of the Panticosa-Western Cauterets Plutons showing the location, the unsuccessful identification performance of the EGMS viewer and kinematic status of RGs based on LiDAR and InSAR data processed by the SqueeSAR software. (B) LiDAR surface change map and LOS displacement rate in ascending and descending orbits of Argualas RG.

provided by the EGMS viewer.

5.1. Panticosa-Western Cauterets plutons

A total of 34 small RGs, predominantly oriented towards the north, northeast, or northwest, were mapped, covering a surface area of 14.3 km^2 (Fig. 3A). SqueeSAR identified 7 RGs as relict, 18 as inactive, 1 as possibly active (Argualas RG), and 8 as active (Fig. 3A; Table 1, Supplementary material). These findings contrast with previous kinematic studies (Serrano et al., 2011; Ventura, 2016), which classified only 4 RGs as active. However, InSAR data revealed that 2 of these 4 RGs had been previously misinterpreted and are now considered inactive.

The Argualas RG (Figs. 3B and 4), characterized by its tongue-shaped morphology, is the only one lacking InSAR measurement points but is considered possibly active due to its fresh appearance, altitude, orientation and geodetic studies (Serrano et al., 2006). It is situated within a deep cirque excavated in Devonian limestones and slates, surrounded by peaks exceeding 3000 m in elevation. Previous studies using resistivity profiles and total station measurements (Serrano et al., 2006) between 1991 and 2000 indicated that the internal structure of the Argualas RG consists of a frozen core 10 to 20 m thick, beneath 4 m of unfrozen debris. These measurements showed mean annual horizontal and vertical motion rates of 20–40 cm/yr and up to 16 cm/yr, respectively, with significant temporal variations, particularly increasing during warmer years. These movement rates are too high for InSAR and consequently, as noted, neither the SqueeSAR algorithm nor the EGMS viewer provides surface motion data of this RG (Fig. 2B). However, a comparison of the two LiDAR datasets in 10-year period (2010−2020) reveals significant surface changes along the Z axis. No positive values, indicative of glacier advance due to creep, were observed. In contrast, negative values associated with frost melting and subsidence (Zahs et al., 2019) were recorded in the frontal, central, and root areas, ranging from −10 to −25 cm/yr, with the greatest subsidence along the central axis. These lowering values and surface changes are consistent with data recorded by Serrano et al. (2006) and confirms the melting tendency and the rapid thinning of the frozen body visible since 1991.

All active RGs are small, moraine-type, and oriented towards the north or northwest (Fig. 3A and Table 1, Supplementary material). They are located at elevations above 2340 m and exhibit well-defined arcuate ridges and furrows, devoid of vegetation. The largest RGs, Cambales and Serrato, are tongue-shaped and oriented to the north, with surface areas of 90,000 m^2 and 70,000 m^2, and frontal elevations exceeding 2400 m and 2600 m, respectively (Figs. 3A and 4). These RGs are situated at the base of steep headwalls, excavated in monzogranites and diorites, respectively, and are covered by talus slopes and cones. The SqueeSAR ground surface velocities along the radar line of sight (LOS) in both ascending and descending geometries reveals a similar kinematic pattern in these two RGs (Fig. 5). The central and upper portions exhibit

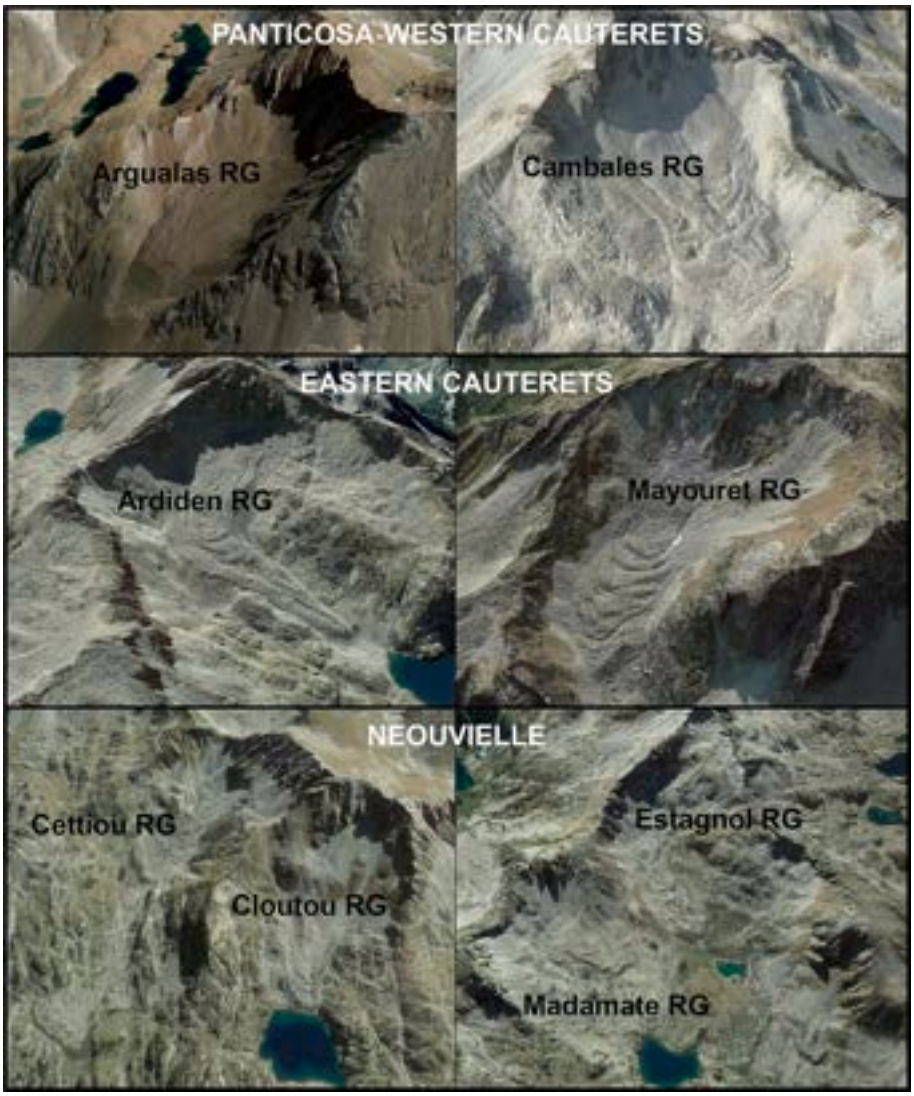

Fig. 4. Google Earth images of active RG in the Pyrenees exhibiting well-defined arcuate ridges and furrows. Notice the retreat of RGs in the Neouvielle massif.

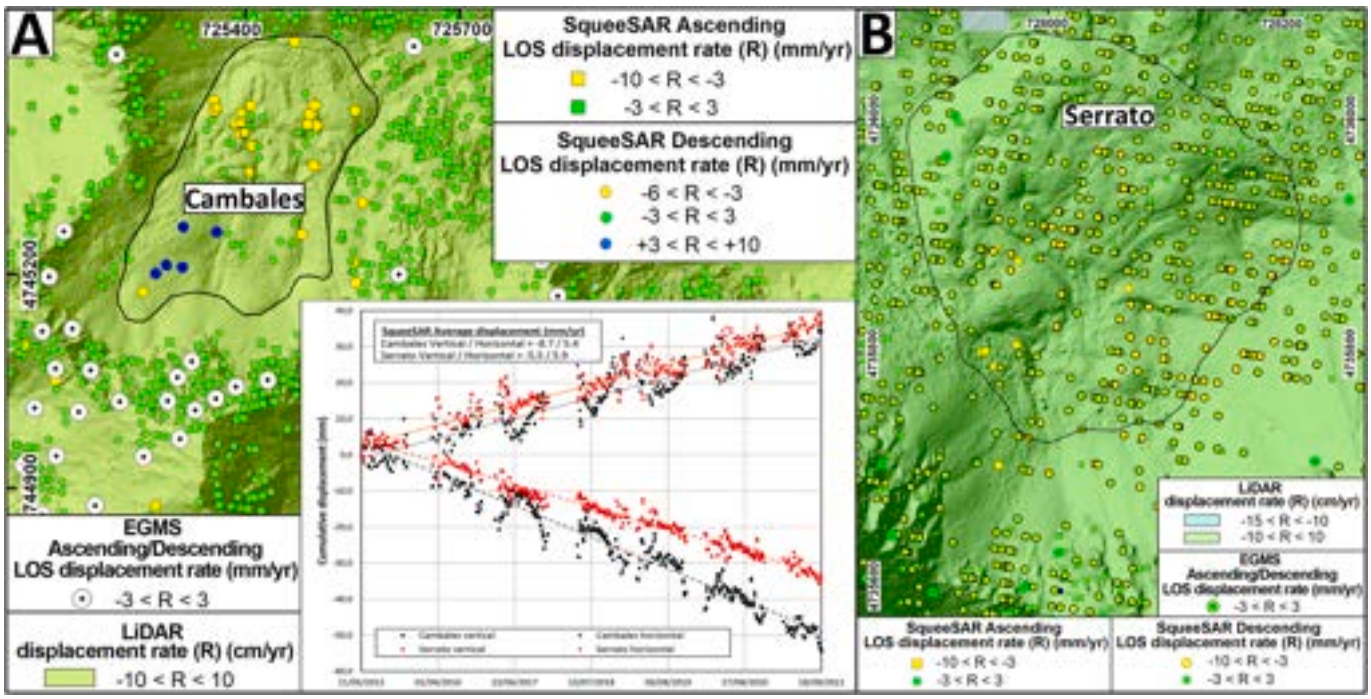

Fig. 5. LiDAR surface changes, LOS displacement rates in ascending and descending geometries and decomposed vertical and horizontal displacement rates of Cambales (A) and Serrato (B) RGs.

very low decomposed vertical and horizontal average displacement rates of −8.4/5.4 mm/yr for Cambales and − 5.5/5.9 mm/yr for Serrato, respectively. In contrast, their frontal sections show negligible velocities and are no longer in motion. These minimal creeping rates are consistent with deformation rates of less than 10 mm/yr in the decomposed horizontal and vertical components calculated for the remaining active RGs in the massif (Table 1, Supplementary material). The Time Series of deformation (TS) for Serrato RG shows a similar linear cumulative deformation trend in the decomposed vertical and horizontal components, suggesting continuous downslope creep at very low rates since 2015 (Fig. 5). In the case of Cambales RG, there is marked seasonal variation of its surface velocity with increasing displacement values in the summer. In contrast, the Lavasa, Piniecho, Punta Puerto, and Xuans RGs display low negative decomposed vertical displacement values and horizontal movement rates close to the detection error margin of ±3 mm/yr, indicating little to negligible downslope movement (Fig. 3A and Table 1; Supplementary material).

The EGMS only provides ground information for 3 out of 34 RGs (2 inactive and 1 relict) and fails to detect any active RGs (Fig. 3A), including Cambales and Serrato (Fig. 5). Similarly, the comparison of LiDAR point clouds did not reveal statistically significant surface changes for any of the active RGs (Fig. 5). This is consistent with their very low rates of movement, which are well below the detection threshold of 10 cm/yr for airborne LiDAR dataset comparison.

5.2. Eastern Cauterets pluton

We have identified a total of 51 RGs, 33 moraine-type and 18 talus-type. They are above 2100 m high and display variable surface areas from less than 5000 to more than 200,000 m^2, 83 % are facing N, NE or NW slopes and 85 % are developed in acid igneous rocks. The SqueeSAR ground deformation maps suggests that 23 out of 51 are still active which represent 45 % of the total and 22 more than the previous inventory. In addition, 19 (37 %) and 9 (18 %) out of 51 are inactive and relict, respectively. The majority of the active RGs are located along two granodioritic ridges separated by the Lutour river (Fig. 6A). These are mainly north-oriented and show a remarkable fresh-looking topography with deep furrows and ridges independently of the moraine or talus typology (Table 2, Supplementary material). Nevertheless, those RGs located at altitudes lower than 2100 m are already partly colonized by bushes and small trees in response to climate warming and tree line rising in the Pyrenees (Camarero et al., 2015).

The decomposed vertical and horizontal SqueeSAR velocity maps show a consistent kinematic trend across all active RGs in the massif. Decomposed vertical displacement values, ranging from −3 to −13 mm/yr and indicative of subsidence or northward displacement, are observed almost uniformly across the entire area of each RG, even at their head (Fig. 7 and Fig. 1 and Table 2, Supplementary material). The maximum negative decomposed vertical displacement occurs at the root zones, gradually decreasing along the slope, becoming negligible at the fronts where the frozen bodies or interstitial ice have completely disappeared. Only Mayouret (Fig. 4), Des Batans, Cestrede and Lit Loungue RGs, with average decomposed vertical velocities around −11 mm/yr, continue to exhibit displacement at their fronts suggesting the persistence of surface ice throughout their entire areas (Fig. 7, Fig. 1, Supplementary material). Probably, the Moraine-type Ardiden (Fig. 4) and Bastampe RGs characterized by prominent and apparently active surface morphologies, also retain an underlying frozen core across their entire extent. However, their north-facing orientation, high altitude and long-lasting snow cover result in image decorrelation, limiting InSAR data to isolated deformation points on their flanks where sidewall friction reduces ground displacement (Fig. 7). Consequently, the kinematic status of these RGs remains incomplete, and their displacement rates should be regarded as minimum estimates. The decomposed horizontal motion displays a spatial pattern similar to that of the vertical component, with maximum values (3 to 33 mm/yr; Table 2, Supplementary material) concentrated in the root zones and minimal or absent displacement at the fronts (ie: Lazahare RG, Fig. 5B and C). Additionally, the InSAR-derived time series (TSs) of displacement exhibit a constant slope, indicative of slow and continuous decomposed vertical and horizontal movements, supporting a steady downslope creep since 2015 across all RGs in the massif (Fig. 1, Supplementary material). It is worth mentioning that Badet RG is the only active RG facing southeast (Figs. 6A and 7, right panel). This talus-type RG, located between 2560

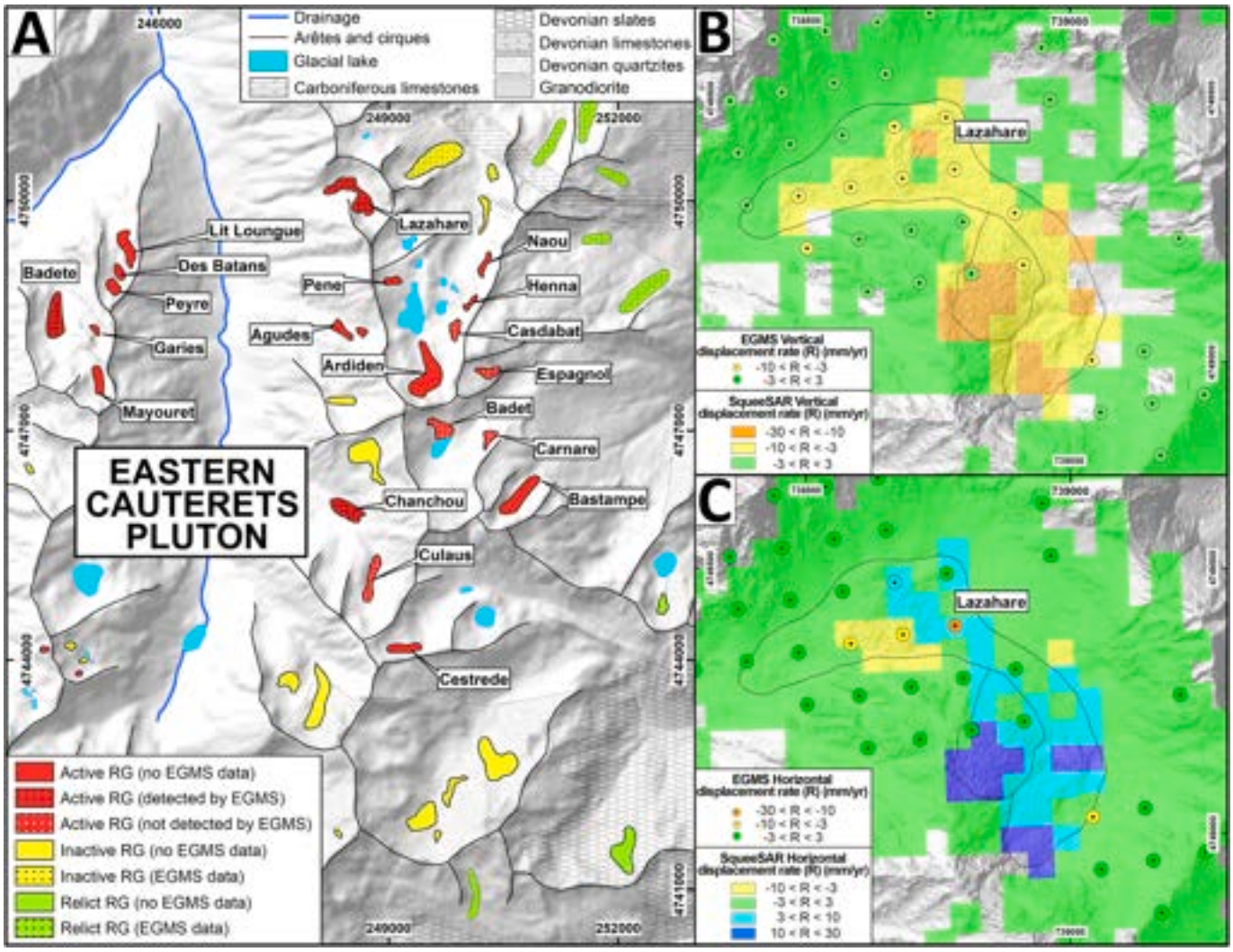

Fig. 6. A) Geological sketch of the Eastern Cauterets Pluton displaying the location, and the kinematic status of RGs based on InSAR data processed by the SqueeSAR software and the EGMS. (B-C) Decomposed vertical and horizontal velocity maps of the Lazahare RG derived from the SqueeSAR algorithm and the EGMS viewer.

and 2660 m high terminates into and advances forward a glacier lake. The serial analysis of old and recent aerial images evidences that the RG tongue and the lake shoreline have not experienced significant changes since 1956 supporting its slow or absent front advance (Fig. 2. Supplementary material). This finding is corroborated by the SqueSAR ground deformation maps, which record an inactive front and decomposed vertical and horizontal displacements confined to the root zone above 2600 m (Fig. 7).

The EGMS viewer provides ground deformation points of 14 RGs out of 51 which means that only 23 % of the RGs have displacement information (Fig. 6A). However, among those 14, 5 active RGs are classified as inactive (Active RG not detected by EGMS in Fig. 6A) which yields a classification error rate of 35 %. In detail, this online InSAR platform identifies 7 out of 9 relict (77 % detection rate), 5 out of 19 inactive (26 % detection rate) and only 3 (Badete, Chanchou and Lazahare) active RGs out of 23 (13 % detection rate) (Fig. 7). The comparison of the decomposed vertical and horizontal EGMS deformation points and SqueeSAR raster velocity maps of the latter RGs evidence that the EGMS platform is not able to register the complete spatial distribution of the deformation detecting surface changes in less than 50 % of the RGs aerial surfaces mainly due to a lack of ground points at their heads in all the cases (Figs. 6B, C and 7). Besides, the long-term average displacement TSs from the decomposed vertical and horizontal components (Fig. 8A and B) demonstrate that EGMS viewer provides similar deformation slopes and cumulative displacement values for Chanchou RG but a shallower motion line and up to 4 times lower average velocities for Lazahare RG than the ones obtained by SqueeSAR. In the case of Badete RG, the EGMS viewer does not give data for the descending orbit but yields an ascending LOS average velocity of −5.7 mm/yr which is less than half of the one recorded by SqueeSAR (−12.4 mm/yr). Both the EGMS and SqueeSAR record surface velocity changes over a year with an increasing displacement trend in the warmer seasons for Lazahare, Chanchou, Badete, (Fig. 8) and Ardiden, Badet and Bastampe (Fig. 1, Supplementary material).

5.3. Neouvielle pluton

The photointerpretation conducted in this study allows updating the inventory to 105 RGs which are mainly located at the northern part of the pluton (Fig. 9) covering a surface area of 9.1 km^2. The SqueeSAR data analysis suggests that 32 are still active, 47 are inactive and 22 are relict. In addition, 3 north-facing RGs have not PS or DS for their kinematic classification and are considered to be possibly active based on their fresh-looking ridge and furrow surface topography, high altitude situation and lack of vegetation. Most of the active ones are moraine-type (23 out of 32; 71 %), developed in igneous acid rocks (31 out of 32; 96 %) and facing north (27 out of 32; 85 %) with only 3 facing South (Contade RG), Southeast (Pic Bastan) or Southwest (Bastan RG).

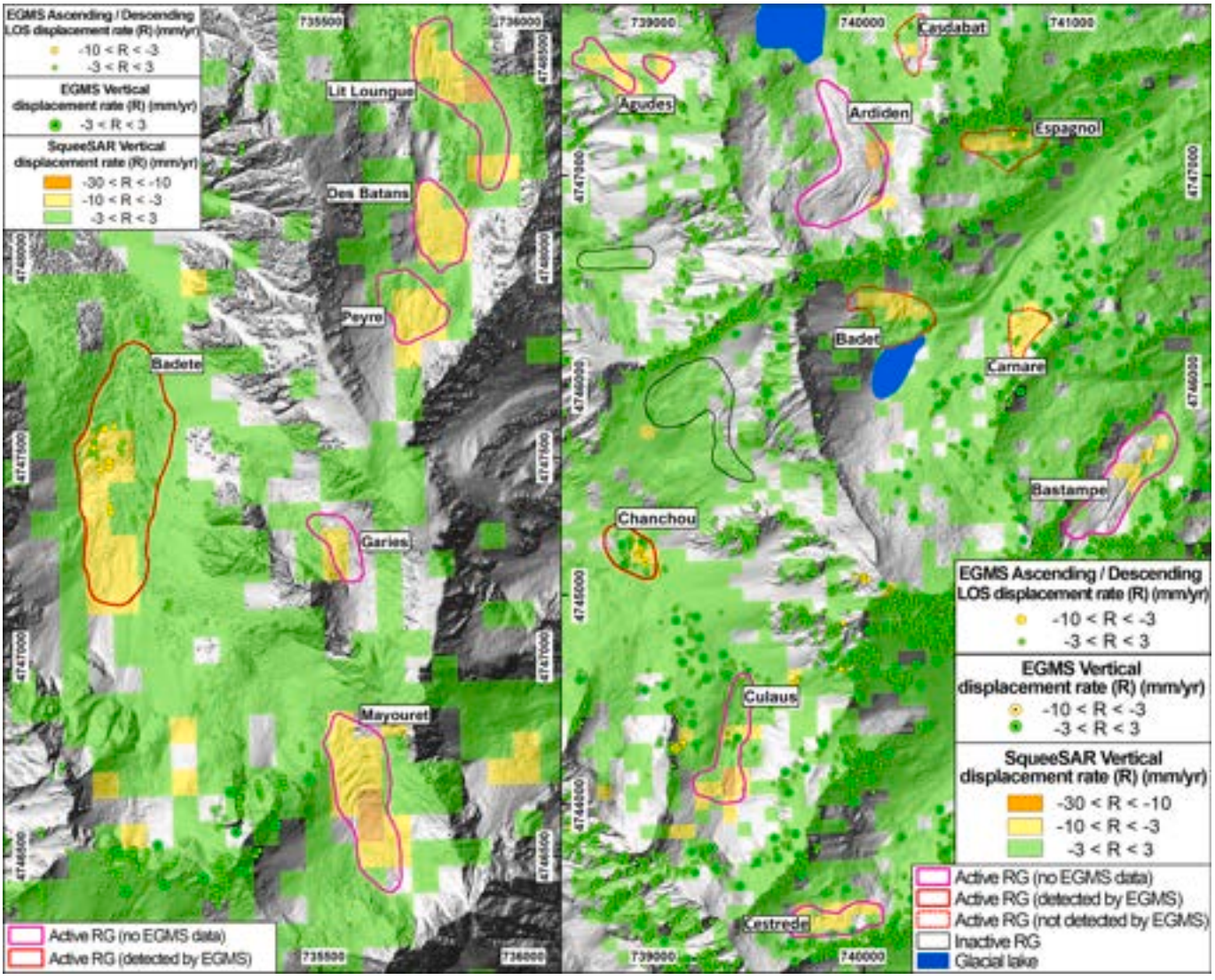

Fig. 7. Decomposed vertical displacement maps generated using SqueeSAR software and vertical and LOS displacement rates in ascending and descending orbits derived from the EGMS viewer for the western (left) and eastern ridges (right) of the Eastern Cauterets pluton.

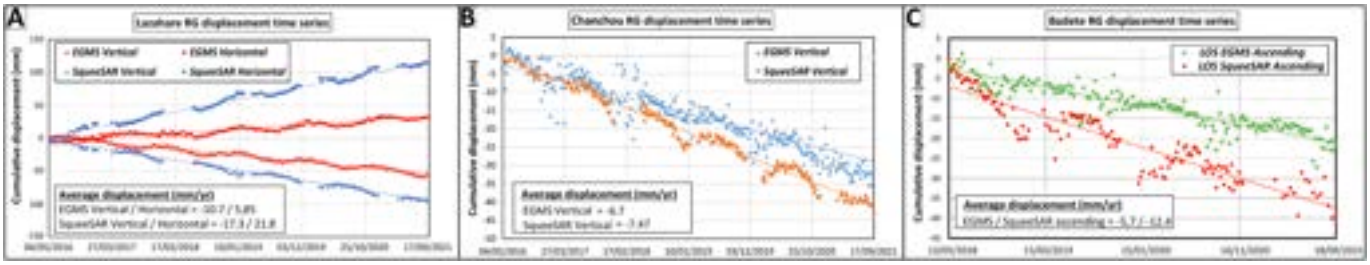

Fig. 8. TS graphs showing the differences in the decomposed vertical and horizontal average displacement for Lazahare and Chanchou and LOS average displacement for Badete RGs obtained by the SqueeSAR software and the EGMS viewer.

Regarding their altitudinal distribution, the SqueeSAR ground deformation maps register movement in RGs located at relatively low heights above 2100 and 2400 in north-oriented and south-oriented slopes, respectively.

The westernmost sector holds the largest, active, talus-type RGs of the pluton which are developed at a deep glacial valley excavated into two granodioritic aretes situated at 2700–2500 m in altitude (Fig. 9). Fig. 10 shows the location and ground velocities of 5 RGs located in this sector. The talus-type and northeast facing Lurtet, Touatere and Tracens and the debris-type and north-facing Estagnol and Madamate RGs (Fig.4) show a similar surface change pattern (Fig. 10 and Table 3, Supplementary material). Image photointerpretation and the InSAR ground displacement maps evidence that all their fronts are no longer moving since they are already partially or fully eroded by the drainage network and colonized by the vegetation. Only their heads at their contact with their feeding talus cones register deformation. Here, the

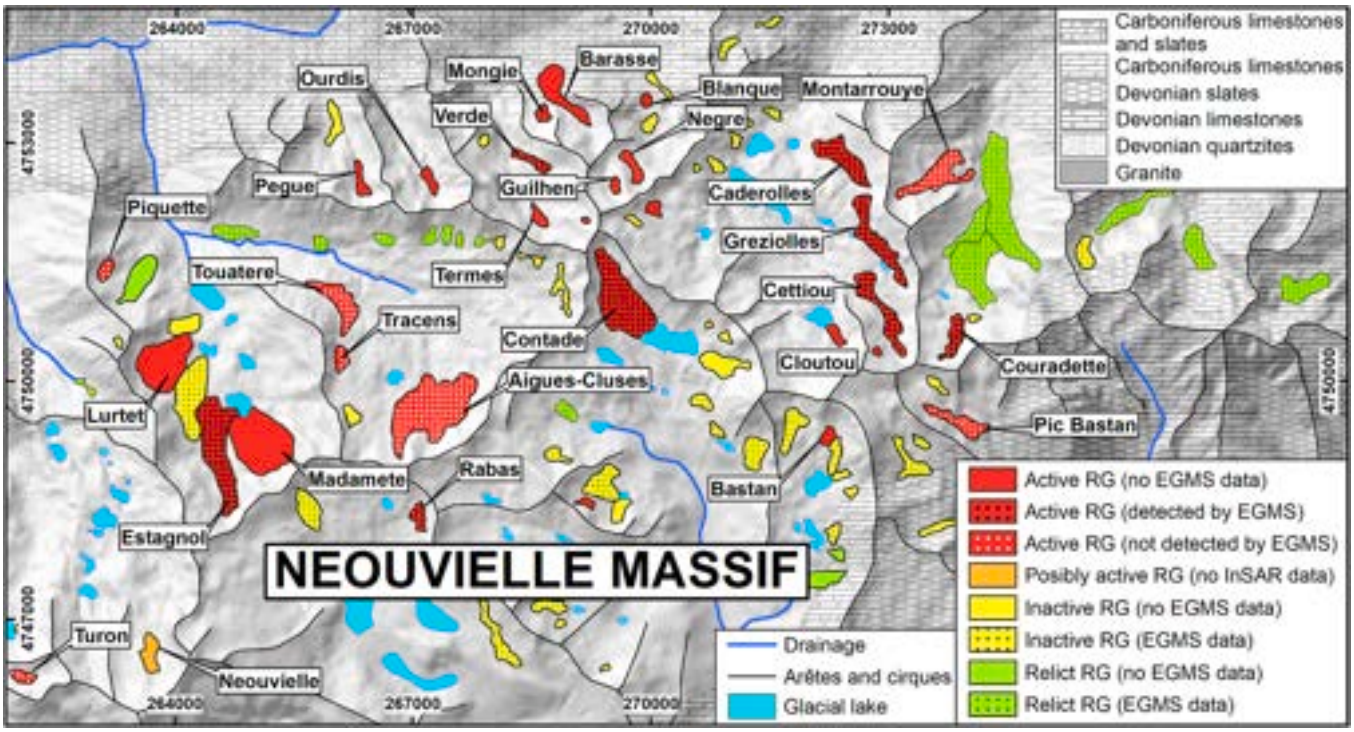

Fig. 9. Geological sketch of the Neouvielle Pluton displaying the location and the kinematic status of RGs based on InSAR data processed by the SqueeSAR software and the EGMS.

decomposed vertical velocities are always negative ranging from −13 to −19 mm/yr related to surface lowering and positive decomposed horizontal velocities between 4 and 16 mm/yr, indicating flow movement in the east direction. The TS of deformation show a linear trend with a steady slope in the decomposed vertical and horizontal components without significant changes with time (Fig. 10).

In contrast to the westernmost sector, the central area of the Neouvielle Pluton is characterized by a significant concentration of active, small, debris-type RGs situated at elevations exceeding 2150 m, predominantly at the base of narrow cirques with subvertical headwalls (Fig. 9). Most of these RGs are oriented towards the north or northwest, with the exception of the Contade RG, the only active glacier facing southeast (Fig. 11). In this context, flow velocities are distinctly influenced by orientation. North-facing RGs typically exhibit movement across nearly their entire surface, while northwest-oriented RGs display immobile fronts with deformation limited to their central and upper sections. In contrast, south- or southeast-facing RGs are either relict or inactive, apart from the Contade RG, which shows deformation above 2400 m along the north-facing cirque headwall slope. Notably, the surface velocities of RGs are more strongly correlated with elevation than with orientation. Those with root zones located above 2500 m, such as Contade and Negre, exhibit the highest displacement rates, with decomposed vertical and horizontal components exceeding −10 mm/yr and + 10 mm/yr, respectively (Fig. 11 and Table 3, Supplementary material). Below this elevation, flow velocities progressively decrease, with decomposed vertical and horizontal displacement values of approximately −5 mm/yr and + 5 mm/yr, respectively. The RGs situated at the lowest altitudes no longer exhibit decomposed horizontal movement, showing only very low negative decomposed vertical displacement, which indicates that downslope flow has almost ceased pointing to their transition towards inactivity (Table 3; Supplementary material).

In the easternmost sector, there is a reduced number of RGs located on both sides of a north-south trending arête at an elevation of approximately 2500 m (Fig. 9). Here, the InSAR velocity maps reveal a ground deformation pattern similar to that observed in other sectors, with motionless, vegetation-covered, and eroded fronts, as well as negative decomposed vertical velocities ranging from −3 to −12 mm/yr (Fig. 12). Decomposed horizontal flow rates of up to 12 mm/yr are confined to the RGs' head regions and increase with elevation (Fig. 12, Table 3, Supplementary material). In this context, the 1200 m long, debris-type, north-facing Cettiou RG (Fig. 4) exhibits the highest surface velocities, with a decomposed vertical rate of −12.7 mm/yr and a westward flow rate of −12.3 mm/yr.

Based on the SqueeSAR data, the EGMS viewer provides ground data for 42 out of 105 RGs, accounting for 40 % of the total RGs with available displacement information (Fig. 9). To be more precise, this online tool has detected 8 out of 32 active (25 % detection rate), 22 out of 47 inactive (46 % detection rate), and 12 out of 22 relict RGs (54 %). Additionally, it incorrectly categorizes 6 active RGs as inactive (Fig. 8). Similarly, it does not provide detailed information for the entire surface experiencing deformation with a lack of data in the upper root areas close to the headwalls. On the other hand, the comparison of the TSs in the central and westernmost sectors reveals that EGMS reports velocity values that are 1.2 to over 4 times lower than those obtained by the SqueeSAR algorithm. Nevertheless, the error in the deformation rates is minimized for RGs facing west, such as Verde (Fig. 10) and Greziolles (Fig. 12), while it is most pronounced for south- and north-facing RGs, such as Contade (Fig. 11) and Cettiou (Fig. 12), respectively, where the difference in the velocity of displacement can reach a factor of 4. Although this measurement error is evident in both decomposed vertical and horizontal velocities, it is particularly pronounced in the east-west velocity component, yielding negligible deformation values or values very close to the detection threshold limit of the technique in all cases. Finally, the TSs curves derived from the EGMS data exhibit greater dispersion of the measurement points and trendlines with a shallower slope compared to those obtained from SqueeSAR data.

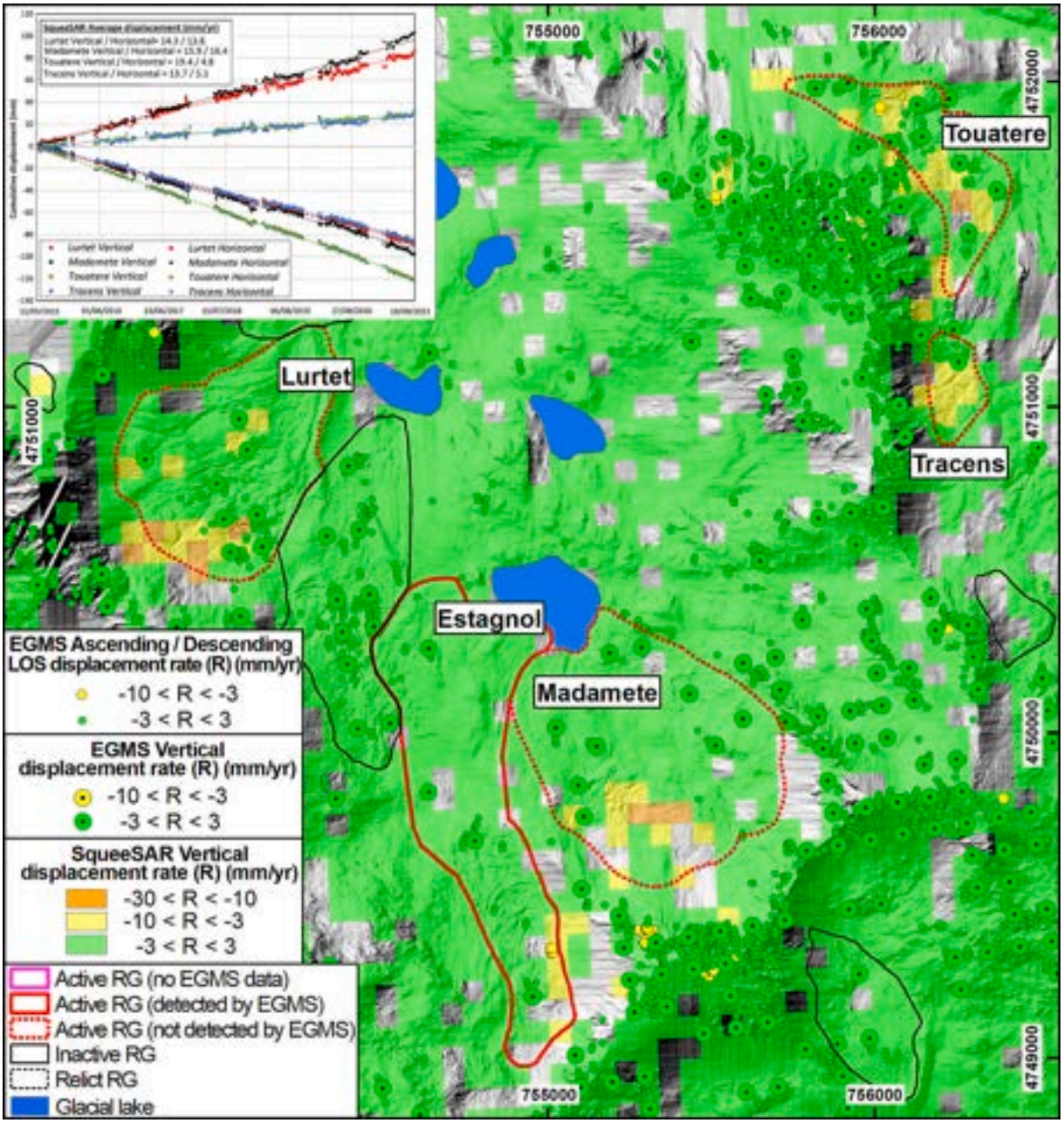

Fig. 10. Decomposed vertical displacement maps generated using SqueeSAR software and vertical and LOS displacement rates in ascending and descending orbits derived from the EGMS viewer for the western side of Neouvielle pluton. The SqueeSAR TSs of Lurtet, Madamate, Touatere and Tracens are displayed in the upper left corner.

6. Discussion

6.1. Inventory of RGs

The integration of Google Earth, high resolution orthoimages and InSAR-derived ground deformation maps, provided by the EGMS viewer and SqueeSAR, has enabled the development of the first kinematic inventory of RGs in the Pyrenees, following the baseline concepts proposed by the International Permafrost Association (IPA) Action Group (RGIK, 2023). This new InSAR inventory, which includes 733 RGs, is significantly more complete than the geomorphic-based databases developed by the Spanish (IGME, 2009) and French (BRGM, 2024) Geological Surveys, and updates previous periglacial studies (Chueca, 1992; Serrano et al., 2011; García-Ruiz et al., 2011; Gómez Ortiz et al., 2011; Fernandes et al., 2017; Fernandes et al., 2023; Ventura, 2016, 2020, and references therein). Building on the most comprehensive geomorphic-based inventory to date, which identified 5 active and 60 possibly active RGs (Ventura, 2016), this new InSAR database significantly increases the number of confirmed active glaciers to 95 and identifies 102 glaciers as possibly active despite the previously mentioned limitations of the EGMS viewer. When combining the active and possibly active glaciers, the total number rises to 197, representing a 258 % increase.

In the Panticosa-Eastern Cauterets pluton, our InSAR inventory identifies 26 previously RGs that were missed in earlier studies (García-Ruiz et al., 2011; Serrano et al., 2011). It also reclassifies 5 RGs previously considered active as inactive and raises the total number of active RGs to 8. In the Eastern Cauterets and Neouvielle plutons, the geomorphological maps developed by the French Geological Survey (BRGM, 2024) do not include any rock glaciers. The earlier inventory by Feuillet

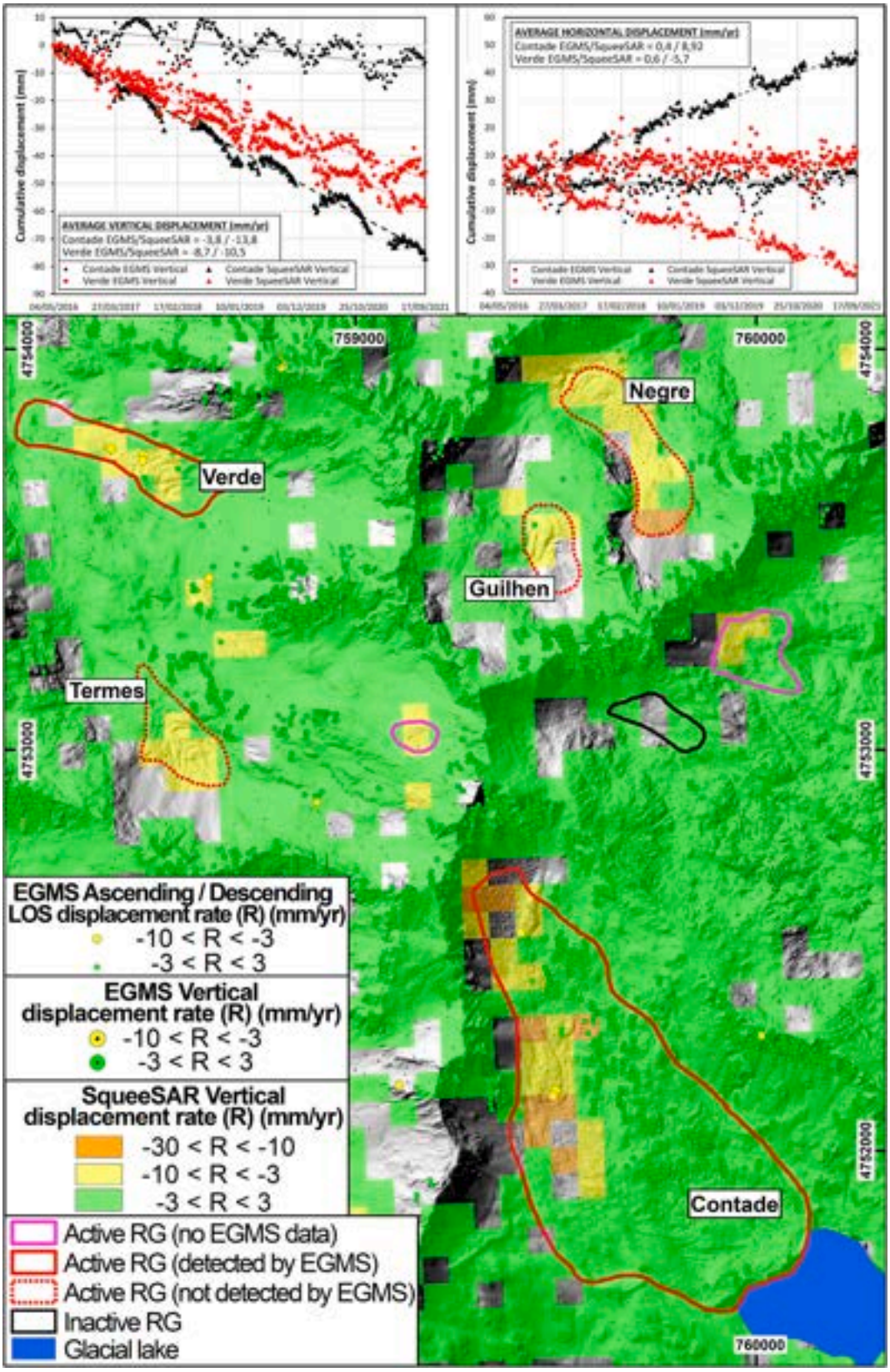

Fig. 11. TS and decomposed vertical displacement maps generated using SqueeSAR software and decomposed vertical and LOS displacement rates in ascending and descending orbits derived from the EGMS viewer for the central section of Neouvielle pluton. The EGMS and SqueeSAR TSs of Contade and Verde are displayed on top showing the great differences in the decomposed vertical and horizontal average displacement rates derived from these two InSAR approaches.

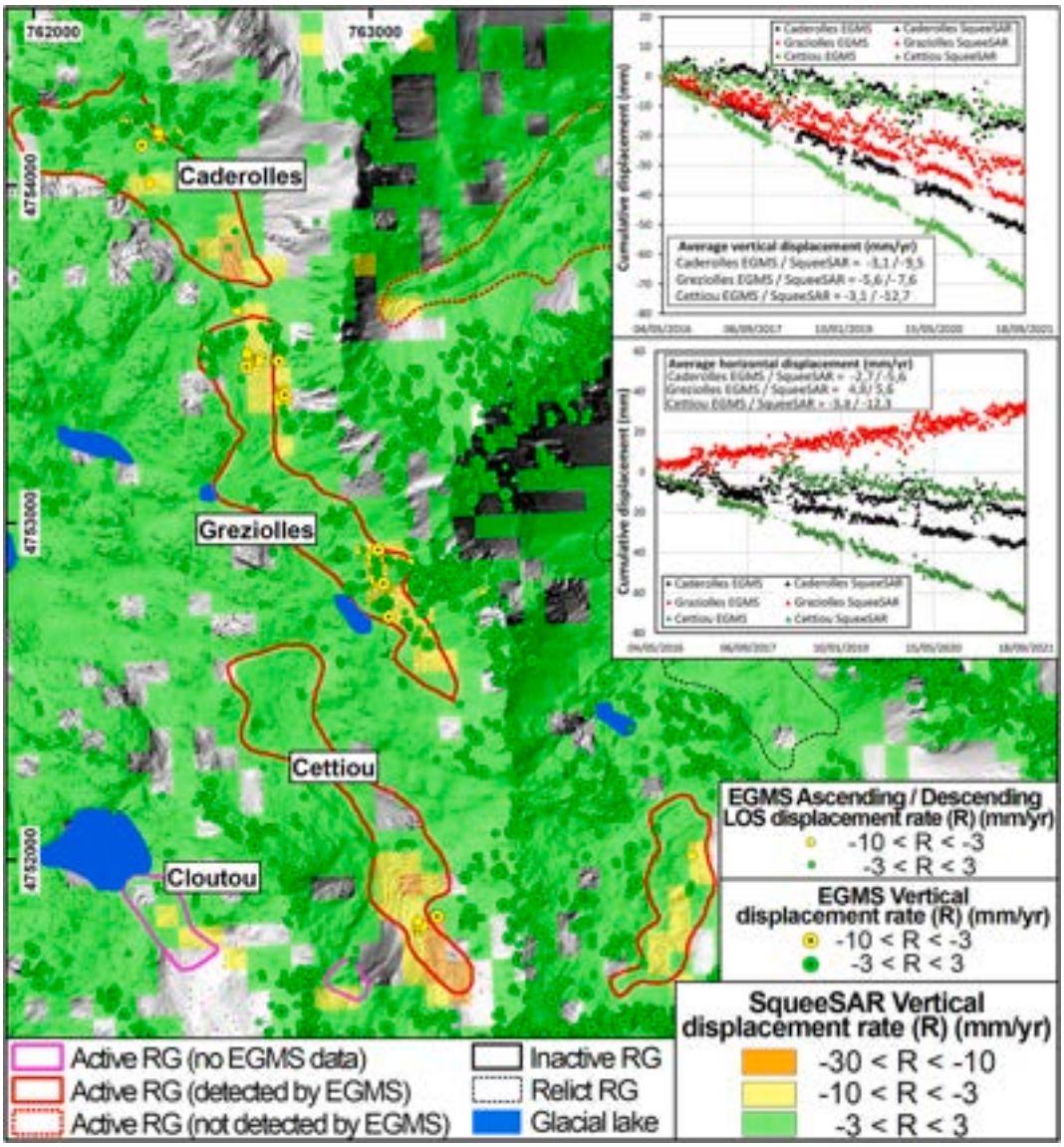

Fig. 12. Decomposed vertical displacement maps generated using SqueeSAR software and vertical and LOS displacement rates in ascending and descending orbits derived from the EGMS viewer for the easternmost area of Neouvielle pluton. The TSs, depicted in the right top corner, exhibit the differences in the decomposed vertical and horizontal average displacement for Caderolles, Greziolles and Cettiou RGs obtained by the SqueeSAR software and the EGMS viewer.

(2010) listed 15 RGs, only 3 of which were classified as active. Subsequently, Ventura (2016) increased the number of active RGs to 9. The integration of photointerpretation and InSAR data has now enabled the identification of 156 RGs, 57 of which are active and 1 possibly active, representing a 1040 % increase in RG identification. These findings align with previous studies (Liu et al., 2013; Wang et al., 2017; Cai et al., 2021; Bertone et al., 2022; Reinosch et al., 2021; Hu et al., 2023) and the IPA guidelines (RGIK, 2023) that highlight the necessity of integrating aerial image interpretation with InSAR techniques to improve the identification of RGs and the quantification of their kinematics.

6.2. Potential and limitations of LiDAR, SqueeSAR and EGMS viewer in RG detection

The integration of SqueeSAR and airborne LiDAR datasets provided essential information on surface kinematics in three granodioritic plutons of the central Pyrenees. Nevertheless, SqueeSAR resulted more efficient than airborne LiDAR to detect active RGs. Airborne LiDAR point cloud comparison has proven to be an extremely useful technique to quantify surface displacement with high accuracy over annual and decadal timescales (Mora et al., 2018; Bataller, 2019; Liu et al., 2019; Guerrero et al., 2021). However, ground measuring and co-registration errors in high alpine areas made this technique only useful for detecting large movements involving important topographic changes. In the study area, the co-registration error between the two datasets allows the confiden detection of RGs with a mean displacement rate threshold over 10 cm/yr. Considering the very low moving rates of Pyrenean RGs, only those with marked surface changes are detected. In contrast, thanks to the exploitation of a large set of interferograms (886 radar images covering 6 years), the surface motion rate threshold limit of SqueeSAR in the study area is 3 mm/yr (Nardini et al., 2024) which is almost one order of magnitude lower than LiDAR, becoming a reliable technique for the detection of slow-moving active RGs. However, the technique has shown several limitations in RG detection and quantification of their surface deformation inherent to InSAR processing (Wang et al., 2017; Bertone et al., 2022; Hu et al., 2023). More specifically, some active RGs could not be detected by SqueeSAR due to coherence loss mainly related to a long-lasting snow cover, their north topographic orientation insensitive to LOS measurements, geometric distortions and their topographic location in shadow areas. In these cases, the use of airborne

LiDAR point cloud comparison helps detect active RGs that lack InSAR kinematic information and are missed due to decorrelation. The advantage of this combined methodology is clearly demonstrated in the Panticosa-Western Cauterets pluton. Here, SqueeSAR provides kinematic information for 8 out of 9 active RGs while airborne LiDAR datasets subtraction only detects 1 out of 9 active RGs, which is, in particular, the one missed by SqueeSAR.

Despite the fact that the EGMS viewer has been confidently used to monitor landslides, subsidence, earthquake and volcanic phenomena all over Europe (Constantini et al., 2021; Sala Calero et al., 2023), the performance of this spaceborne radar database to detect slow-moving active RGs in the Pyrenees has been unsuccessful. In the Panticosa-Western Cauterets pluton only provides ground information for 3 out of 34 RGs (2 inactive and 1 relict) and could not detect any of the active RGs. In the Eastern Cauterets and Neouvielle plutons, the EGMS viewer provides ground data for only 23 % and 40 % of all the RGs, respectively, and is able to detect only 11 out of 55 active RGs. In addition, the kinematic information is erroneous 35 % of the time, does not register the complete spatial distribution of the deformation detecting surface changes in less than 50 % of the RGs surface and gives up to 4 times lower average decomposed vertical and horizontal velocities than the ones reported by SqueeSAR leading to shallower TS cumulative deformation curves.

It is crucial to note that the primary cause of the inefficient detection of RGs and measurement of their ground displacement by the EGMS viewer, as compared to the SqueeSAR approach, lies in the differences in processing strategies. While both methods utilize InSAR displacement data derived from the same Sentinel-1 radar imagery for ascending and descending orbits at full resolution, the EGMS processes all available SAR images over a continuous annual time window, yielding velocity measurements derived from the complete dataset (EGMS, 2017, 2020; Ferretti et al., 2011). In contrast, the SqueeSAR algorithm used in this research has selectively processed radar images acquired exclusively during snow-free periods, mitigating the impact of snow cover and reducing temporal decorrelation (Cai et al., 2021; Guerrero et al., 2021; Huang et al., 2024). This approach is particularly significant in the Pyrenees, where snowfall lasts for approximately five months (December to April), with snow cover thickness reaching 2–3 m. As highlighted in the guidelines of the IPA Action Group (2022; RGIK, 2023) and a large number of recent research papers (e.g. Bertone et al., 2022; Lambiel et al., 2023; Onaca et al., 2025), SAR imagery for RG detection in mountainous regions with prolonged snow cover should primarily be acquired during snow-free periods. Consequently, given the low detection rate of the EGMS platform due to the interferometric decorrelation caused by extended snow cover, the current kinematic assessment of our Pyrenean RG inventory should be considered a preliminary evaluation. Future updates are necessary, employing a processing strategy that relies on radar images covering only the snow-free periods to avoid coherence loss in order to better capture the full range of active RGs in the study area.

6.3. Movement rates of Pyrenean RGs

In this regard, the rate of displacement of Pyrenean RGs is largely unknown and limited to geodetic surveys of 5 large and highly dynamic RGs located in the central Pyrenees. Their monitoring has revealed horizontal and vertical movement rates ranging from 2 to 40 and − 2 to −22 cm/yr, respectively, depending considerably on their altitude, slope, orientation and measuring time and with increasing velocities from their fronts to the head and from the margins to the axis (Serrano et al., 1999; Chueca and Julián, 2005; Serrano et al., 2006, 2010; González-García et al., 2013; de Sanjosé et al., 2014; Martínez-Fernández et al., 2024). GNSS values are in agreement with LiDAR data. In the Panticosa-western Cauterets pluton, the LiDAR negative velocities of Argualas RG is between −10 and − 25 cm/yr in agreement with the geodetic data recorded by Serrano et al. (2006). Likewise, in the eastern central Pyrenees, the elevation difference obtained from the subtraction between two LiDAR derived DEM yield a motion rate for Besiberri RG similar to those reported by GPS data (Chueca and Julián, 2005) and allows Bataller (2019) to identify other four active RGs with average vertical displacement ranging from −8 to −26 cm/yr. Unfortunately, none of the latter RGs have InSAR kinematic data available since they are located in deep north-facing cirques surrounded by vertical walls covered by a persistent snow cover that may last all the year. In addition, the surface displacement maps obtained from GPS and LiDAR surveys cannot be strictly compared with decomposed InSAR datasets. The decomposition of movement into east-west and up-down components, while disregarding the north component of deformation (Bru et al., 2024), may lead to biased estimates, particularly in the up-down component (Brouwer and Hanssen, 2023; Brouwer and Hanssen, 2024). This assumption represents a significant limitation of the technique, especially given that most active RGs in the Pyrenees are predominantly oriented and moving northward. In such cases, the projection of the horizontal displacement of RGs along the north-south axis onto the LOS direction may result in negative values, which could be misinterpreted as subsidence in the decomposed vertical component (Brouwer and Hanssen, 2023, Brouwer and Hanssen, 2024). Consequently, a negative vertical value should not be directly attributed to permafrost degradation and ice thickness lowering since it may arise from the combination of subsidence and horizontal northward displacement. Despite these limitations, there are a large number of active RGs in the study area that could serve as valuable comparisons.

In general, the EGMS and SqueeSAR decomposed horizontal displacement maps display a deformation pattern consistent with the geodetic measurements showing decreasing velocities to the fronts and margins. However, the deformation magnitude is significantly lower than the rates from other techniques. The InSAR decomposed horizontal movement rate of the most active RGs in the Panticosa-Western Cauterets, Eastern Cauterets and Neouvielle varies from 4 to 5, 13 to 21 and 11 to 16 mm/yr, respectively (Tables 1–3, Supplementary material). These averages velocities are one order of magnitude lower than the geodetic measurements. Similarly, decomposed vertical velocities in these plutons range from −5 to −9, −4 to −17 and − 3 to −19 mm/yr which are between 11 and 13 times lower than GNSS values and LiDAR surface changes. Although InSAR deformation results are validated and often in agreement with GNSS data (Rémy et al., 2014; Tizzani et al., 2007; Munroe, 2018), there are also a large number of studies that show significant measurement discrepancies between these two techniques (Bejar-Pizarro et al., 2016; Guerrero et al., 2021; Marshall et al., 2022; Shi et al., 2022). Note that there are several causes that may explain the underestimation of motion in the InSAR time series in our study. Firstly, InSAR and geodetic data do not cover the same temporal period and most important, they are referred to difference RGs. Secondly, InSAR reflects the average deformation over a 5*20 m area, whereas GNSS provides the local deformation of receivers located at specified sites. Finally, considering that InSAR is less sensitive to ground displacement oriented to the north and 81 % of the active RGs are facing North, Northeast or Northwest, the motion rate might be largely underestimated (Klees and Massonnet, 1998; Liu et al., 2013; Wang et al., 2017; Bertone et al., 2022). According to the guidelines of the IPA Action Group (RGIK, 2023), the underestimation of InSAR data on ground displacement has significant consequences for the classification of RGs, depending on the measurement technique used. Based on InSAR velocity maps, all active Pyrenean RGs could be classified as “transitional” from active to inactive, with average displacement rates of less than 10 cm/year. However, when considering GNSS and LiDAR data, along with the underestimation of ground deformation in InSAR measurements, at least some of them are moving above this threshold and should be classified as “active slow-moving RGs”.

6.4. Permafrost distribution in the Pyrenees

Active RGs (Serrano et al., 1999; Chueca and Julián, 2005; Serrano et al., 2006, 2010; González-García et al., 2013; de Sanjosé et al., 2014; Martínez-Fernández et al., 2024), patterned grounds and frost mounds (Feuillet, 2010; Feuillet and Mercier, 2012; Serrano et al., 2019, 2020) and ice caves (Sancho et al., 2018; Serrano et al., 2018; Bartolomé et al., 2022), are reliable indicators of the occurrence and spatial distribution of frozen ground in the Pyrenees. Based on the altitudinal distribution of these landforms and thermal ground recordings, previous studies establish the lower limit for the presence of permafrost above 2650 m on north-facing slopes and 2900 m on south-facing slopes (Serrano et al., 2019; Oliva et al., 2023). Excluding potentially active RGs and focusing solely on the active RGs from the current kinematic inventory, the altitudinal boundary of frozen ground in the Pyrenees appears to be lower than previously reported, with significant differences between north- and south-facing slopes. In this line, SqueeSAR ground deformation maps record movement in RGs situated at relatively low elevations, over 2100 m and 2600 m in the Eastern Cauterets pluton and over 2150 and 2400 m in the Neouvielle plutons, on north- and south-facing slopes, respectively. These altitudinal values lower the permafrost limit around 500 m on both north- and south-facing slopes than the ones previously reported (Serrano et al., 2019, 2020; Rico et al., 2021; Oliva et al., 2023). This is supported by the monitoring studies of the basal temperatures of the snow cover south of the Panticosa Massif where permafrost appeared to exist at points between 1900 and 2400 ma.s.l., especially within the avalanche tracks (Julián and Chueca, 2007). Nevertheless, caution must be exercised when interpreting a direct relationship between active RGs and the regional permafrost limit. Numerous studies have documented cases of sporadic permafrost or so-called ‘cold spots’ on talus slopes, characterized by frozen ground and temperatures considerably lower than those of adjacent soil or bedrock (Niu et al., 2016 and references therein). Therefore, the presence of active RGs at low altitudes may simply reflect the irregular distribution of sporadic permafrost (Serrano et al., 2020), driven by local steep topographic conditions that reduces solar radiation and promotes the persistence of snow cover (Julián and Chueca, 2007). However, the substantial number of active RGs observed at low elevations above 2100 m suggests the need to revise downward the currently established lower limit of permafrost in the Pyrenees.

Notably, the altitudinal distribution of active RGs in the three studied granodioritic plutons varies markedly depending on the orientation in the range. In the Panticosa-Western Cauterets pluton, located at the southern side of the range, active RGs are over 2340 m. In contrast, in the Eastern Cauterets pluton and Neouvielle plutons, located at the northern side of the range, SqueeSAR ground deformation maps record movement in RGs situated at relatively low elevations over 2100–2150 m, respectively. This 200–250-m decrease in the permafrost limit in the Eastern Cauterets and Neouvielle plutons, is explained by their 3–4 °C lower average annual temperature and 500–1000 mm greater precipitation (Feuillet, 2010) than the Panticosa massif. Consequently, periglacial processes are expected to be more active in the north-facing plutons even at lower altitudes.

Although the number of active RGs decreases towards the east as peak elevation and rainfall diminish, surprisingly, the altitudinal limit of active RGs does not change significantly from west to east. In fact, the easternmost granitic massif (L’Infern-Canigó massif) hosts several active RGs above 2300–2400 m as in the Panticosa massif in the central Pyrenees where rainfall rate is almost double, highlighting the importance of local topographic factors in the occurrence of permafrost.

Finally, the decomposition of the InSAR deformation into decomposed vertical and horizontal velocities from the ascending and descending geometries provides additional information than the downslope velocities (projection of the LOS velocity field into the slope direction) derived from a single orbit. In particular, most of the RGs in the Pyrenees show low to negligible decomposed horizontal movement at their fronts and all display negative decomposed vertical values probably related to a combination of subsidence and northward displacement in their entire surface. The reduction in their decomposed horizontal displacement rates and the lowering values recorded by the SqueeSAR and EGMS viewer are clear signs of their transition from active to relict due to the thinning of their ice content. In addition, the drainage erosion of the fronts and tongues, a smoother surface topography, and the rapid colonization of their fronts by vegetation support ice content decline. The linear slope of the cumulative negative decomposed vertical velocities visible in the TS graphs might suggest that ice loss processes have been continuous since 2015 in agreement with previous GPS studies and LiDAR data that record a steady subsidence related to ice degradation since the beginning of the century (Chueca and Julián, 2005; Serrano et al., 2006, 2010; González-García et al., 2013; de Sanjosé et al., 2014). If this trend continues in the near future, as expected from the presented rapid permafrost degradation signs, the marked temperature increase recorded recently (López-Moreno et al., 2019) and the significant decline of snow depth at elevations above 2000 m a.s.l. (López-Moreno, 2005; López-Moreno et al., 2020; Vidaller et al., 2021), the number of active RGs in the Pyrenees will dramatically decrease in the recent years.

7. Conclusions

The integration of SqueeSAR and airborne LiDAR datasets in this study has demonstrated significant potential for detecting and quantifying surface kinematics of RGs in the Pyrenees, albeit with notable limitations. SqueeSAR proved to be more effective than airborne LiDAR for identifying slow-moving active RGs, with a motion detection threshold of 3 mm/year, almost an order of magnitude lower than LiDAR’s threshold. Despite this, SqueeSAR’s performance is hindered by factors such as coherence loss, snow cover, and topographic orientation, leaving certain RGs undetected. Airborne LiDAR, although less sensitive to smaller displacements, complemented SqueeSAR by detecting RGs in areas with poor InSAR coherence, demonstrating the strength of a combined methodological approach.

The EGMS viewer, despite its success in monitoring other geohazards, was ineffective in detecting slow-moving RGs in the Pyrenees. The low detection rate, combined with significant errors in the kinematic data provided, underscores the need for a different strategy that relies on radar images covering only the snow-free periods to avoid coherence loss to update the kinematic status of RGs in future studies.

The newly developed InSAR-based RG inventory for the Pyrenees, which identifies 733 RGs, marks a substantial improvement over previous geomorphic databases. This inventory highlights a significant increase in the identification of active RGs, suggesting that the combined use of InSAR techniques and aerial photointerpretation is critical for enhancing the accuracy of RG inventories.

However, discrepancies between InSAR and geodetic measurements, particularly in movement rates, highlight the need for caution in interpreting kinematic data. InSAR tends to underestimate RG motion, especially for north-facing slopes, which could lead to misclassification of active RGs as transitional. This study calls for further refinement of InSAR techniques to ensure more accurate monitoring of RG dynamics, particularly as permafrost degradation accelerates in response to ongoing climate change.

In terms of permafrost distribution, this study presents evidence of lower altitudinal limits for active RGs than previously reported although further detailed investigations are required to establish the spatial and altitudinal distribution of continuous, discontinuous and sporadic permafrost, and to determine whether active RGs located at very low elevations represent “cold spots”. In any case, these findings suggest significant variability in permafrost occurrence between north- and south-facing slopes, with topographic and climatic factors playing a crucial role. The ongoing degradation of permafrost, coupled with reduced snow cover and rising temperatures, is expected to lead to a

dramatic decline in the number of active RGs in the Pyrenees in the coming years.

Author contribution

All the authors participated in editing and reviewing the manuscript. J.G., T.Y., and G.D. were mainly responsible for the mapping of RGs. J.G. and MG were in charge of the acquisition and processing of the Squee-SAR and EGMS InSAR velocity maps. J.G. and B.C., participated in the production of maps and contributed significantly to collecting and interpreting the data. All authors have read and agreed to the published version of the manuscript.

Funding

This research has been supported by the European Union Interreg VI-A España-Francia-Andorra (Poctefa 2021–2027), project SPIRAL EFA039/01. M.G. has a research contract financed by the European Union.

Declaration of competing interest

The authors declare the following financial interests/personal relationships which may be considered as potential competing interests:

Jesus Guerrero Iturbe reports financial support was provided by European Union. If there are other authors, they declare that they have no known competing financial interests or personal relationships that could have appeared to influence the work reported in this paper.

Appendix A. Supplementary data

Supplementary data to this article can be found online at https://doi.org/10.1016/j.rse.2025.114798.

Data availability

The authors do not have permission to share data.

References

Andrés, N., Gómez-Ortiz, A., Fernández-Fernández, J.M., Tanarro, L.M., Salvador-Franch, F., Oliva, M., Palacios, D., 2018. Timing of deglaciation and rock glacier origin in the southeastern Pyrenees: a review and new data. Boreas 47, 1050–1071. https://doi.org/10.1111/bor.12324. ISSN 0300-9483.

Barnolas, A., Pujalte, V., 2004. La cordillera Pirenaica. Geología de España, SGE-IGME, Madrid, pp. 233–241.

Barsch, D., 1992. Permafrost creep and rockglaciers. Permafr. Periglac. Process. 3, 175–188. https://doi.org/10.1002/PPP.3430030303.

Bartolomé, M., Cazenave, G., Luetscher, M., Spötl, C., Gázquez, F., Belmonte Ribas, Á., Turchyn, A., López-Moreno, J., Moreno, A., 2022. Mountain permafrost in the Central Pyrenees: insights from the Devaux ice cave. EGU. https://doi.org/10.5194/egusphere-2022-349.

Bataller, F., 2019. Pyrenaic rock glaciers: an airborne and multitemporal LiDAR monitoring case study in the Besiberri area. EarthArXiv. https://doi.org/10.31223/osf.io/nxveh.

Bejar-Pizarro, M., Guardiola-Albert, C., García-Cárdenas, R., Herrera, G., Barra, A., Molina, A., Tessitore, S., Staller, A., Ortega-Becerril, J., García-García, R., 2016. Interpolation of GPS and geological data using InSAR deformation maps: method and application to land subsidence in the alto Guadalentín aquifer (SE Spain). Remote Sens. 8, 965. https://doi.org/10.3390/rs8110965.

Berthling, I., 2011. Beyond confusion: rock glaciers as cryoconditioned landforms. Geomorphology 131, 98–106. https://doi.org/10.1016/J.GEOMORPH.2011.05.002.

Bertone, A., Barboux, C., Bodin, X., Bolch, T., Brardinoni, F., Caduff, R., Christiansen, H., Darrow, M., Delaloye, R., Etzelmüller, B., Humlum, O., Lambiel, C., Lilleøren, K., Mair, V., Pellegrinon, G., Rouyet, L., Ruiz, L., Strozzi, T., 2022. Incorporating InSAR kinematics into rock glacier inventories: insights from 11 regions worldwide. Cryosphere 16, 2769–2792. https://doi.org/10.5194/tc-16-2769-2022.

BRGM, 2024. Infoterre-Web portal for access to BRGM scientific data. https://infoterre.brgm.fr/ (accessed 09 November 2024).

Brouwer, W.S., Hanssen, R.F., 2023. A treatise on InSAR geometry and 3D displacement estimation. IEEE Trans. Geosci. Remote Sens. 61. https://doi.org/10.1109/TGRS.2023.3322595. Article 5217811.

Brouwer, W.S., Hanssen, R.F., 2024. Estimating three-dimensional displacements with InSAR: the strapdown approach. J. Geod. 98, 1–15. https://doi.org/10.1007/s00190-024-01918-2.

Bru, G., Ezquerro, P., López Vinielles, J., Reyes-Carmona, C., Guardiola-Albert, C., Bejar-Pizarro, M., 2024. Manual básico sobre el uso de datos InSAR para medir desplazamientos de la superficie del terreno. CSIC. https://doi.org/10.13039/501100011033.

Cai, J., Wang, X., Liu, G., Yu, B., 2021. A comparative study of active rock glaciers mapped from geomorphic-and kinematic-based approaches in Daxue Shan, southeast Tibetan plateau. Remote Sens. 13, 4931. https://doi.org/10.3390/rs13234931.

Camarero, J., García-Ruiz, J.M., Sangüesa-Barreda, G., Galván, J., Alla, A., Sanjuan, Y., Beguería, S., Gutiérrez, E., 2015. Recent and intense dynamics in a formerly static Pyrenean Treeline. Arct. Antarct. Alp. Res. 47, 773–783. https://doi.org/10.1657/AAAR0015-001.

Campos, N., Alcalá, J., Watson, C.S., Kougkoulos, I., Quesada-Román, A., Grima, N., 2021. Modelling the retreat of the Aneto glacier (Spanish Pyrenees) since the little ice age, and its accelerated shrinkage over recent decades. Holocene 31. https://doi.org/10.1177/09596836211011678.

Cazenave-Piarrot, F., Tihay, J.P., 1983. Eboulis, formations morainiques et glaciers rocheux dans le massif de l'Ardiden (Pyrénées centrales). In: Soutade, G., Barthelemy, L. (Eds.), Eboulis et environnement géographique passé et actuel. Association les amis du centre de géographie physique Henri Elhaï, Nanterre, pp. 121–135.

Cazenave-Piarrot, F., Tihay, J.P., 1986. Glaciers rocheaux dans les Pyrénées Centrales et Occidentales. Communication a la Societé Hydrotechnique de France (section Glaciologie), Paris, p. 8.

Chueca, J., 1992. A statistical analysis of the spatial distribution of rock glaciers, Spanish Central Pyrenees. Permafr. Periglac. Process. 3, 261–265. https://doi.org/10.1002/ppp.3430030316.

Chueca, J., Julián, A., 2005. Movement of Besiberris rock glacier, Central Pyrenees, Spain: data from a 10-year geodetic survey. Arct. Antarct. Alp. Res. 37, 163–170. https://doi.org/10.1657/1523-0430(2005)037[0163:MOBRGC]2.0.CO;2.

Colesanti, C., Ferretti, A., Locatelli, R., Novali, F., Savio, G., 2003. Permanent scatterers: precision assessment and multi-platform analysis. In: IGARSS 2003. 2003 IEEE international geoscience and remote sensing symposium, Proceedings, July 2003, 2. IEEE cat. No. 03CH37477, Toulouse, France, pp. 1193–1195. https://doi.org/10.1109/IGARSS.2003.1294055.

Colucci, R.R., Boccali, C., Žebre, M., Guglielmin, M., 2016. Rock glaciers, protalus ramparts and pronival ramparts in the South-Eastern Alps. Geomorphology 269, 112–121. https://doi.org/10.1016/j.geomorph.2016.06.039.

Constantini, M., Minati, F., Trillo, F., Ferretti, A., Novali, F., Passera, E., Dehls, J., Larsen, Y., Marinkovic, P., Eineder, M., Brcic, R., Siegmund, R., Kotzerke, P., Probeck, M., Kenyeres, A., Proietti, S., Solari, L., Andersen, H., 2021. European ground motion service (EGMS): general description, product quality, and examples. IEEE Int. Geosci. Remote Sens. Symp. 2021, 3293–3296. https://doi.org/10.1109/IGARSS47720.2021.9553562.

Crosetto, M., Solari, L., Mróz, M., Balasis-Levinsen, J., Casagli, N., Frei, M., Oyen, A., Moldestad, D.A., Bateson, L., Guerrieri, L., Comerci, V., Andersen, H.S., 2020. The evolution of wide-area DInSAR: from regional and National Services to the European ground motion service. Remote Sens. 12, 2043. https://doi.org/10.3390/rs12122043.

Crosetto, M., Solari, L., Balasis-Levinsen, J., Bateson, L., Casagli, N., Frei, M., Oyen, A., Moldestad, D.A., Mróz, M., 2021. Deformation monitoring at European scale: the Copernicus ground motion service. Int. Arch. Photogramm. Remote. Sens. Spat. Inf. Sci. 141–146. https://doi.org/10.5194/isprs-archives-XLIII-B3-2021-141-2021. XLIII-B3-2021.

de Sanjosé, J.J., Berenguer, F., Atkinson, A.D.J., De Matías, J., Serrano, E., Gómez-Ortiz, A., González-García, M., Rico, I., 2014. Geomatics techniques applied to glaciers, rock glaciers, and ice patches in Spain (1991–2012). Geogr. Ann. Ser. A Phys. Geogr. 96, 307–321. https://doi.org/10.1111/geoa.12047.

Del Barrio, G., Creus, J., Puigdefábregas, J., 1990. Thermal seasonality on the high mountain belts of the Pyrenees. Mt. Res. Dev. 10 (3), 227–233. https://doi.org/10.2307/3673602.

EGMS, 2017. White Paper. https://land.copernicus.eu/en/products/european-ground-motion-service/d2_d3_combined_sip_psd-1_01_final-1.pdf/@@download/file (accessed 14 May 2024).

EGMS, 2020. EGMS Implementation Plan and Product Specification Document. https://land.copernicus.eu/user-corner/technical-library/egms-white-paper accessed 14 May 2024.

EGMS, 2023. European Ground Motion Service Explorer. https://egms.land.copernicus.eu/ accessed 12 September 2024.

Fernandes, M., Palma, P., Lopes, L., Ruiz Fernández, J., Pereira, P., Oliva, M., 2017. Spatial distribution and morphometry of permafrost-related landforms in the Central Pyrenees and associated paleoclimatic implications. Quat. Int. 470. https://doi.org/10.1016/j.quaint.2017.08.071.

Fernandes, M., Oliva, M., Fernández-Fernández, J., Vieira, G., García Oteyza, C., Ventura, J., Schimmelpfennig, I., Team, A., 2023. Geomorphological record of the glacial to periglacial transition from the Bølling-Allerød to the Holocene in the Central Pyrenees: the Lòcampo cirque in the regional context. Boreas 53. https://doi.org/10.1111/bor.12633.

Ferretti, A., Fumagalli, A., Novali, F., Prati, C., Rocca, F., Rucci, A., 2011. A new algorithm for processing interferometric data-stacks: SqueeSAR. IEEE Trans. Geosci. Remote Sens. 49 (9), 3460–3470. https://doi.org/10.1109/TGRS.2011.2124465.

Ferretti, A., Passera, E., Capes, R., 2021. Algorithm theoretical basis document. EGMS Doc. https://land.copernicus.eu/user-corner/technical-library/egms-algorithm-theoretical-basis-document (accessed 1 March 2024).

Feuillet, T., 2010. Les formes périglaciaires dans les Pyrénées centrales françaises: analyse spatiale, chronologique et valorisation. PhD Thesis. Université de Nantes. https://theses.hal.science/tel-00564112. accessed 17 September 2024.

Feuillet, T., Mercier, D., 2012. Post-little ice age patterned ground development on two Pyrenean proglacial areas: from deglaciation to periglaciation. Geogr. Ann. Ser. A Phys. Geogr. 94, 363–376. https://doi.org/10.1111/j.1468-0459.2012.00459.x.

Galé, C., 2005. Evolución geoquímica, petrogenética y de condiciones geodinámicas de los magmatismos pérmicos en los sectores central y occidental del Pirineo. PhD Thesis,. Universidad de Zaragoza, p. 457.

García-Ruiz, J.M., Peña Monné, J.L., Marí-Bono, C., Gómez-Villar, A., Espinalt, M., 2011. El relieve del Alto Aragón Occidental. Cartografía y síntesis geomorfológica. Consejo de Protección de la Naturaleza de Aragón, Zaragoza, p. 91.

García-Ruiz, J.M., Palacios, D., Andrés, N., Valero-Garcés, B., López-Moreno, J.I., Sanjuan, Y., 2014. Holocene and 'little ice age' glacial activity in the Marbore cirque, Monte Perdido massif, central Spanish Pyrenees. Holocene 24, 1439–1452. https://doi.org/10.1177/0959683614544053.

Gil, A., Lago, M., Gale, C., Anchuela, O., Ubide, T., Tierz, P., Oliva, B., 2012. The Permian mafic dyke swarm of the Panticosa pluton (Pyrenean axial zone, Spain), simultaneous emplacement with the late-Variscan extension. J. Struct. Geol. 42, 171–183. https://doi.org/10.1016/j.jsg.2012.05.008.

Gleizes, G., Leblanc, D., Olivier, P., Bouchez, J., 2001. Strain partitioning in a pluton during emplacement in transpressional regime: the example of the Néouvielle granite (Pyrenees). Int. J. Earth Sci. 90, 325. https://doi.org/10.1007/s005310000144.

Gómez Ortiz, A., Franch, F., Oliva, M., Salva Catarineu, M., 2011. Morfología glaciar y periglaciar de la Cerdanya (Pirineo Oriental): los sectores de Aränser-La Llosa y la Feixa-La Màniga. XIII Reunión Nacional de Cuaternario, Simposio de glaciarismo. AEQUA.

González-García, M., Serrano, E., Sanjosé Blasco, J.J., González Trueba, J.J., 2013. Surface dynamic and current status of the Madaleta rock glacier (Pyrenees). Cuad. Investig. Geogr. 37, 81–94.

González-García, M., Serrano, E., Sanjosé, J.J., González-Trueba, J.J., 2016a. Surface dynamic of a protalus lobe in the temperate high mountain. Maladeta, Western Pyrenees. Catena 149, 689–700. https://doi.org/10.1016/j.catena.2016.08.011.

González-García, M., Serrano, E., González-Trueba, J.J., 2016b. Morphogenesis, morphodynamic and thermal definition of frost mounds in the Pyrenees (Maladeta and Posets massifs). Polígonos 28, 73–93. https://doi.org/10.18002/pol.v0i28.4288.

Guerrero, J., Sevil Aguareles, J., Desir, G., Gutiérrez, F., García-Arnay, Á., Galve, J., Reyes-Carmona, C., 2021. The detection of active sinkholes by airborne differential lidar dems and Insar cloud computing tools. Remote Sens. 13, 3261. https://doi.org/10.3390/rs13163261.

Hu, Y., Liu, L., Huang, L., Zhao, L., Wu, T., Wang, X., Cai, J., 2023. Mapping and characterizing rock glaciers in the arid Western Kunlun Mountains supported by InSAR and deep learning. J. Geophys. Res. Earth 128. https://doi.org/10.1029/2023JF007206 e2023JF007206.

Huang, C., Wang, L., Zhao, L., Liu, S., Zou, D., Liu, G., Hu, G., Erji, D., Xiao, Y., Wang, C., Zhang, Y., Wang, Y., Zhang, Y., Li, Z., 2024. Potential of C-band Sentinel-1 InSAR for ground surface deformation monitoring in the southern boreal forest: an investigation in the Genhe River basin. Int. J. Appl. Earth Obs. Geoinf. 135, 104302. https://doi.org/10.1016/j.jag.2024.104302.

IGME, 2009. Mapa geomorfológico de España a escala 1:50.000. Instituto Geológico y Minero de España. https://info.igme.es/cartografiadigital/tematica/Geomorfologico50.aspx?language=es. accessed: 14 October 2024.

Johnson, G., Chang, H., Fountain, A., 2021. Active rock glaciers of the contiguous United States: geographic information system inventory and spatial distribution patterns. Earth Syst. Sci. Data 13, 3979–3994. https://doi.org/10.5194/essd-13-3979-2021.

Jones, D.B., Harrison, S., Anderson, K., Betts, R.A., 2018. Mountain rock glaciers contain globally significant water stores. Sci. Rep. 8 (2834). https://doi.org/10.1038/s41598-018-21244-w.

Julián, A., Chueca, J., 2007. Permafrost distribution from BTS measurements (sierra de Telera, Central Pyrenees, Spain): assessing the importance of solar radiation in a mid-elevation shaded mountainous area. Permafr. Periglac. Process. 18, 137. https://doi.org/10.1002/ppp.576.

Klees, R., Massonnet, D., 1998. Deformation measurements using SAR interferometry: potential and limitations. Geol. Mijnb. 77, 161–176. https://doi.org/10.1023/A:1003594502801.

Lague, D., Brodu, N., Leroux, J., 2013. Accurate 3D comparison of complex topography with terrestrial laser scanner: application to the Rangitikei canyon (NZ). ISPRS J. Photogramm. Remote Sens. 82, 10–26. https://doi.org/10.1016/j.isprsjprs.2013.04.009.

Lambiel, C., Strozzi, T., Paillex, N., Vivero, S., Jones, N., 2023. Inventory and kinematics of active and transitional rock glaciers in the southern Alps of New Zealand from Sentinel-1 InSAR. Arct. Antarct. Alp. Res. 55, 2183999. https://doi.org/10.1080/15230430.2023.2183999.

Lemirre, B., Cochelin, B., Duchene, S., Blanquat, M.S., Poujol, M., 2019. Origin and duration of late orogenic magmatism in the foreland of the Variscan belt (Lesponne-Chiroulet-Neouvielle area, French Pyrenees). Lithos 336-337, 183–201. https://doi.org/10.1016/j.lithos.2019.03.037.

Lilleøren, K.S., Etzelmüller, B., Rouyet, L., Eiken, T., Hilbich, C., 2022. Transitional rock glaciers at sea-level in northern Norway. Earth Surf. Dynam. 10, 975–996. https://doi.org/10.5194/esurf-2022-6.

Liu, L., Millar, C.I., Westfall, R.D., Zebker, H.A., 2013. Surface motion of active rock glaciers in the Sierra Nevada, California, USA: inventory and a case study using InSAR. Cryosphere 7 (4), 1109–1119. https://doi.org/10.5194/tc-7-1109-2013.

Liu, W., Yamazaki, F., Maruyama, Y., 2019. Detection of earthquake-induced landslides during the 2018 Kumamoto earthquake using multitemporal airborne Lidar data. Remote Sens. 11, 2292. https://doi.org/10.3390/rs11192292.

Lorite Martínez, S., Ojeda, J.C., Rodríguez-Cuenca, R., González, E., Muñoz, P. (2016). Point cloud distribution and processing of the PNOA-LiDAR Project, http://pnoa.ign.es/PNOAtheme/images/imgPNOA/contenidos/pdf/Procesado_distribucion_nubes_puntos_proyecto_PNOA-LiDAR.pdf (accessed on 14 June 2024).

López-Moreno, J.I., 2005. Recent variations of snowpack depth in the central Spanish Pyrenees. Arct. Antarct. Alp. Res. 37, 253–260. https://doi.org/10.1657/1523-0430(2005)037[0253:RVOSDI]2.0.CO;2.

López-Moreno, J.I., Alonso-González, E., Monserrat, O., del Río, L.M., Otero, J., Lapazaran, J., Luzi, G., Dematteis, N., Serreta, A., Rico, I., Serrano-Cañadas, E., Bartolomé, M., Moreno, A., Buisan, S., Revuelto, J., 2019. Ground-based remote-sensing techniques for diagnosis of the current state and recent evolution of the Monte Perdido glacier, Spanish Pyrenees. J. Glaciol. 65, 85–100. https://doi.org/10.1017/jog.2018.96.

López-Moreno, J.I., Soubeyroux, J.M., Gascoin, S., Alonso-Gonzalez, E., Durán-Gómez, N., Lafaysse, M., Morin, S., 2020. Long-term trends (1958–2017) in snow cover duration and depth in the Pyrenees. Int. J. Climatol. 40 (14), 6122–6136. https://doi.org/10.1002/joc.6571.

Marshall, C., Sterk, H., Pieter, G., Peter, J., Andersen, R., Bradley, A., Sowter, A., Marsh, S., Large, D., 2022. Multiscale variability and the comparison of ground and satellite radar based measures of peatland surface motion for peatland monitoring. Remote Sens. 14, 336. https://doi.org/10.3390/rs14020336.

Martinez de Pison, E., Lopez-Martinez, J., Duran, J., 1998. Rock Glaciers in the Pyrenees, Spain and France, Version 1. NSIDC: National Snow and Ice Data Center, Boulder, Colorado USA. https://doi.org/10.7265/k65d-mg83.

Martínez-Fernández, A., Serrano, E., de Sanjosé Blasco, J.J., Gómez-Lende, M., Sánchez-Fernández, M., Pisabarro, A., Atkinson, A., 2024. Multiple close-range Geomatic techniques for the kinematic study of the La Paúl rock glacier, southern Pyrenees. Remote Sens. 16, 134. https://doi.org/10.3390/rs16010134.

Mora, O., Lenzano, M., Toth, C., Grejner-Brzezinska, D., Fayne, J., 2018. Landslide change detection based on multi-temporal airborne LIDAR-derived DEMs. Geosciences 8, 23. https://doi.org/10.3390/geosciences8010023.

Munroe, J.S., 2018. Distribution, evidence for internal ice, and possible hydrologic significance of rock glaciers in the Uinta Mountains, Utah, USA. Quat. Res. 90, 50–65. https://doi.org/10.1017/qua.2018.24.

Muñoz, J.A., 2002. The Pyrenees, in: W. Gibbons, T. Moreno (Eds.), The Geology of Spain, Geological Society, London, UK (2002), pp. 370-385.

Nardini, O., Confuorto, P., Intrieri, E., Poggi, F., Raspini, F., Montalti, R., Montanaro, T., Robles, J., 2024. Integration of satellite SAR and optical acquisitions for the characterization of the Lake Sarez landslides in Tajikistan. Landslides 21, 1–17. https://doi.org/10.1007/s10346-024-02214-y.

Niu, F., Cheng, G., Niu, Y., Zhang, M., Luo, J., Lin, Z., 2016. A naturally-occurring 'cold earth' spot in northern China. Sci. Rep. 6, 34184. https://doi.org/10.1038/srep34184.

Notti, D., Herrera, G., Bianchini, S., Meisina, C., García-Davalillo, J.C., Zucca, F., 2014. A methodology for improving landslide PSI data analysis. Int. J. Remote Sens. 35, 2186–2214. https://doi.org/10.1080/01431161.2014.889864.

Oliva, M., Ruiz-Fernández, J., Barriendos, M., Benito, G., Cuadrat, J.M., Domínguez-Castro, F., García-Ruiz, J.M., Giralt, S., Gómez-Ortiz, A., Hernández, A., López-Costas, O., López-Moreno, J.I., López-Sáez, J.A., Martínez-Cortizas, A., Moreno, A., Prohom, M., Saz, M.A., Serrano, E., Tejedor, E., Trigo, R., Valero-Garcés, B., Vicente-Pandey, P., 2019. Inventory of rock glaciers in Himachal Himalaya, India using high-resolution Google earth imagery. Geomorphology 340, 103–115. https://doi.org/10.1016/j.geomorph.2019.05.001.

Oliva, M., Serrano, E., López-Moreno, N., Ventura, J., Echeverria, A., Turu, V., Grau, O., 2023. Towards improving permafrost monitoring in the Pyrenees. In: European Conference on Permafrost, Puigcerda, 10.13140/RG.2.2.33410.66247.

Onaca, A., Sirbu, F., Poncos, V., Hilbich, C., Strozzi, T., Urdea, P., Popescu, R., Berzescu, O., Etzelmüller, B., Vespremeanu-Stroe, A., Vasile, M., Teleagă, D., Birtaş, D., Lopătiță, I., Filhol, S., Hegyi, A., Ardelean, F., 2025. Slow-moving rock glaciers in marginal periglacial environment of southern Carpathians. EGUsphere [Preprint]. https://doi.org/10.5194/egusphere-2024-3262.

OPCC, 2024. Past and Present Climate in the Pyrenees. The Pyrenees Climate Change Observatory. https://www.opcc-ctp.org/en/sector/past-and-present-climate.

Palacios, D., Andrés, N., López-Moreno, J.I., García-Ruiz, J.M., 2015. Late Pleistocene deglaciation in the upper Gállego valley, Central Pyrenees. Quat. Res. 83, 397–414. https://doi.org/10.1016/j.yqres.2015.01.010.

Palacios, D., García-Ruiz, J.M., Andrés, N., Schimmelpfennig, I., Campos, N., Leanni, L., Aumaıtre, G., Bourles, D.L., Keddadouche, K., 2017. Deglaciation in the Central Pyrenees during the Pleistocene-Holocene transition: timing and geomorphological significance. Quat. Sci. Rev. 162, 111–127. https://doi.org/10.1016/j.quascirev.2017.03.007.

Pandey, P., 2019. Inventory of rock glaciers in Himachal Himalaya, India using high-resolution Google Earth imagery. Geomorphology 340. https://doi.org/10.1016/j.geomorph.2019.05.001.

Reinosch, E., Gerke, M., Riedel, B., Schwalb, A., Ye, Q., Buckel, J., 2021. Rock glacier inventory of the western Nyainqêntanglha range, Tibetan plateau, supported by InSAR time series and automated classification. Permafr. Periglac. Process. 32 (4), 657–672. https://doi.org/10.1002/ppp.2117.

Rémy, D., Froger, J.L., Perfettini, H., Sylvain, B., Gabalda, G., Albino, F., Cayol, V., Legrand, D., De, M., de Saint Blanquat, M., 2014. Persistent uplift of the Lazufre volcanic complex (Central Andes): new insights from PCAIM inversion of InSAR time series and GPS data 2. Geochem. Geophys. Geosyst. 15. https://doi.org/10.1002/2014GC005370.

RGIK, 2023. Guidelines for Rock Glacier Inventories: Baseline and Practical Concepts (Version 1.0). IPA Rock Glacier Inventories and Kinematics Action Group, p. 25. https://doi.org/10.51363/unifr.srr.2023.002.

Rico, I., 2019. Los glaciares de los Pirineos. Estudio glaciológico y dinámica actual en el contexto del cambio global. PhD Thesis,. Universidad del País Vasco. https://addi.ehu.es/handle/10810/33085.

Rico, I., Magnin, F., López Moreno, J.I., Serrano, E., Alonso-González, E., Revuelto, J., Hughes-Allen, L., Gómez-Lende, M., 2021. First evidence of rock wall permafrost in the Pyrenees (Vignemale peak, 3,298ma.S.L., 42° 4616N/0° 0833W). Permafr. Periglac. Process. 32, 673–680. https://doi.org/10.1002/ppp.2130.

Sala Calero, J., Vöge, M., Esteves Martins, J., Raucoules, D., de Michelle, M., Vradi, A., Vecchiotti, F., 2023. EGMS Validation Report. https://land.copernicus.eu/en/technical-library/validation-report-2015-2021-dataset/@@download/file accessed: 23 November 2024.

Sancho, C., Belmonte, Á., Bartolomé, M., Moreno, A., Leunda, M., López-Martínez, J., 2018. Middle-to-late Holocene palaeoenvironmental reconstruction from the A294 ice-cave record (Central Pyrenees, northern Spain). Earth Planet. Sc. Lett. 484, 135–144. https://doi.org/10.1016/j.epsl.2017.12.027.

Santana Torre, V.J., 2002. El plutón de Panticosa (pirineos occidentales, Huesca): fábrica magnética y modelo de emplazamiento. Rev. Soc. Geol. Esp. 15 (3–4), 175–191.

Serrano, E., López-Martínez, J., 2000. Rock glaciers in the South Shetland Islands, Western Antarctica. Geomorphology 35 (1–2), 145–162. https://doi.org/10.1016/S0169-555X(00)00034-9.

Serrano, E., Agudo, C., Martínez de Pisón, E., 1999. Rock glaciers in the Pyrenees. Permafr. Periglac. Process. 10, 101–106. https://doi.org/10.1002/(SICI)1099-1530(199901/03)10:13.0.CO;2-U.

Serrano, E., San José, J.J., Agudo, C., 2006. Rock glacier dynamics in a marginal periglacial High Mountain environment: flow, movement (1991–2000) and structure of the Argualas rock glacier, the Pyrenees. Geomorphology 74, 285–296. https://doi.org/10.1016/j.geomorph.2005.08.014.

Serrano, E., de Sanjosé, J.J., González-Trueba, J.J., 2010. Rock glacier dynamics in marginal periglacial environments. Earth Surf. Process. Landf. 35, 1302–1314. https://doi.org/10.1002/esp.1972.

Serrano, E., González Trueba, J.J., San José, J.J., 2011. Dinámica, evolución y estructura de los glaciares rocosos de los Pirineos. Cuad. Invest. Geogr. 37, 145–170.

Serrano, E., Gómez-Lende, M., Belmonte, Á., Sancho, C., SánchezBenítez, J., Bartolomé, M., Leunda, M., Moreno, A., Hivert, B., Per, S.A., 2018. In: Lauritzen, S.E. (Ed.), Chapter 28- ice caves in Spain. Elsevier, Ice Caves, pp. 625–655. https://doi.org/10.1016/B978-0-12-811739-2.00028-0.

Serrano, E., de Sanjosé-Blasco, J.J., Gómez-Lende, M., LópezMoreno, J.I., Pisabarro, A., Martínez-Fernández, A., 2019. Periglacial environments and frozen ground in the central Pyrenean high mountain area: ground thermal regime and distribution of landforms and processes. Permafr. Periglac. Process. 30, 292309. https://doi.org/10.1002/ppp.2032.

Serrano, E., López-Moreno, J.I., Gómez-Lende, M., Pisabarro, A., Martín-Moreno, R., Rico, I., Alonso-González, E., 2020. Frozen ground and periglacial processes relationship in temperate high mountains: a case study at Monte Perdido-Tucarroya area (the Pyrenees, Spain). J. Mt. Sci. 17, 1013–1031. https://doi.org/10.1007/s11629-019-5614-5.

Sevil Aguareles, J., Benito Calvo, A., Gutiérrez, F., 2021. Sinkhole subsidence monitoring combining terrestrial laser scanner and high-precision leveling. Earth Surf. Process. Landf. 46. https://doi.org/10.1002/esp.5112.

Shi, X., Zhu, T., Tang, W., Jiang, M., Jiang, H., Yang, C., Zhan, W., Ming, Z., Zhang, S., 2022. Inferring decelerated land subsidence and groundwater storage dynamics in Tianjin–Langfang using Sentinel-1 InSAR. Int. J. Digital Earth 15, 1526–1546. https://doi.org/10.1080/17538947.2022.2122610.

Strozzi, T., Caduff, R., Jones, N., Barboux, C., Delaloye, R., Bodin, X., Kääb, A., Mätzler, E., Schrott, L., 2020. Monitoring rock glacier kinematics with satellite synthetic aperture radar. Remote Sens. 12, 559. https://doi.org/10.3390/rs12030559.

Tizzani, P., Berardino, P., Casu, F., Euillades, P., Manzo, M., Zeni, G., Lanari, R., 2007. Surface deformation of Long Valley caldera and Mono Basin, California, investigated with the SBAS-InSAR approach. Remote Sens. Environ. 108, 277–289. https://doi.org/10.1016/j.rse.2006.11.015.

Turu, V., Peña-Monné, J.L., Cunha, P.P., Jalut, G., Buylaert, J.P., Murray, A.S., Bridgland, D., FaurschouKnudsen, M., Oliva, M., Carrasco, R.M., Ros, X., Turu-Font, L., Ventura Roca, J., 2023. Glacial-interglacial cycles in the south-central and southeastern Pyrenees since ~180 ka (NE Spain-Andorra-S France). Quaternary Research 113, 1–28. https://doi.org/10.1017/qua.2022.68.

Ventura, J., 2016. Identificación e inventario de potenciales glaciares rocosos activos en los Pirineos mediante Fotointerpretación en visores cartográficos 2D y 3D: Primeros resultados. Rev. Geogr. 95. https://doi.org/10.18002/pol.v0i28.4289.

Ventura, J., 2020. Distribución espacial y temporal de glaciares, glaciares cubiertos y glaciares rocosos durante la última deglaciación en el valle de la Bonaigua (Pirineo Central). Cuad. Invest. Geogr. 46, 415–448. https://doi.org/10.18172/cig.4395.

Vidaller, I., Revuelto, J., Izagirre, E., Rojas Heredia, F., Alonso-González, E., Gascoin, S., René, P., Berthier, E., Rico, I., Moreno, A., Serrano, E., Serreta, A., López-Moreno, J., 2021. Toward an ice-Free Mountain range: demise of Pyrenean glaciers during 2011–2020. Geophys. Res. Lett. 48. https://doi.org/10.1029/2021GL094339.

Vidaller, I., Izagirre, E., Luis, R., Alonso-González, E., Rojas Heredia, F., Serrano, E., Moreno, A., López-Moreno, J., Revuelto, J., 2023. The Aneto glacier (Central Pyrenees) evolution from 1981 to 2022: ice loss observed from historic aerial image photogrammetry and recent remote sensing techniques. Cryosphere 17, 3177–3192. https://doi.org/10.5194/tc-2022-261.

Villarroel, C., Tamburini Beliveau, G., Forte, A., Monserrat, O., Morvillo, M., Villarroel, C.D., Tamburini Beliveau, G., Forte, A.P., Monserrat, O., Morvillo, M., 2018. DInSAR for a regional inventory of active rock glaciers in the dry Andes Mountains of Argentina and Chile with Sentinel-1 data. Remote Sens. 10, 1588. https://doi.org/10.3390/rs10101588.

Wagner, T., Pleschberger, R., Kainz, S., Ribis, M., KellererPirklbauer, A., Krainer, K., Philippitsch, R., Winkler, G., 2020. The first consistent inventory of rock glaciers and their hydrological catchments of the Austrian Alps. Austrian J. Earth Sci. 113, 1–23. https://doi.org/10.17738/ajes.2020.0001.

Wang, X., Liu, L., Zhao, L., Wu, T., Li, Z., Liu, G., 2017. Mapping and inventorying active rock glaciers in the northern Tien Shan of China using satellite SAR interferometry. Cryosphere 11 (2), 997–1014. https://doi.org/10.5194/tc-11-997-2017.

White, S., 1976. Rock glaciers and block fields, review and new data. Quat. Res. 6, 77–97. https://doi.org/10.1016/0033-5894(76)90041-7.

Zahs, V., Hämmerle, M., Anders, K., Hecht, S., Sailer, R., Rutzinger, M., Williams, J., Höfle, B., 2019. Multi-temporal 3D point cloud-based quantification and analysis of geomorphological activity at an alpine rock glacier using airborne and terrestrial LiDAR. Permafr. Periglac. Process. 30, 222–238. https://doi.org/10.1002/ppp.2004.

Zalazar, L., Ferri, L., Castro, M., Gargantini, H., Gimenez, M., Pitte, P., Ruiz, L., Masiokas, M., Costa, G., Villalba, R., 2020. Spatial distribution and characteristics of Andean ice masses in Argentina: results from the first National Glacier Inventory. J. Glaciol. 66, 938–949.

Zhang, X., Feng, M., Zhang, H., Wang, C., Tang, Y., Xu, J., Yan, D., Wang, C., 2021. Detecting rock glacier displacement in the Central Himalayas using multi-temporal InSAR. Remote Sens. 13 (23), 4738. https://doi.org/10.3390/rs13234738.